Josephson voltage standards as toolkit for precision metrological applications at PTB

OPEN ACCESS
IOP Publishing
Measurement Science and Technology
Meas. Sci. Technol. **34** (2023) 032001 (22pp)
https://doi.org/10.1088/1361-6501/aca5a5

Topical Review

Josephson voltage standards as toolkit for precision metrological applications at PTB

Stephan Bauer, Ralf Behr*, Jonas Herick, Oliver Kieler, Marco Kraus, Hao Tian, Yoawaret Pimsut and Luis Palafox

Physikalisch-Technische Bundesanstalt (PTB), Bundesallee 100, 38116 Braunschweig, Germany

E-mail: ralf.behr@ptb.de

Received 29 April 2022, revised 18 October 2022
Accepted for publication 24 November 2022
Published 21 December 2022

Abstract

About 60 years after the discovery of the Josephson effect, electrical DC voltage calibrations are routinely performed worldwide—mostly using automated Josephson voltage standards (JVSs). Nevertheless, the field of electrical quantum voltage metrology is still propagating towards AC applications. In the past 10 years the fabrication of highly integrated arrays containing more than 50 000 or even 300 000 junctions has achieved a very robust level providing highly functional devices. Such reliable Josephson arrays are the basis for many novel applications mainly focussing on precision AC measurements for signal frequencies up to 500 kHz. Two versions of quantum AC standards are being employed. Programmable JVS, based on series arrays divided into subarrays, reach amplitudes up to 20 V and usually are used as quantum voltage reference in measurement systems. Pulse driven arrays reach amplitudes up to 1 V or even 4 V and are typically used as Josephson arbitrary waveform synthesizers. This paper summarizes the principal contributions from Physikalisch-Technische Bundesanstalt to the present state of JVS with particular focus on developments for precision metrological applications and our proof-of-concept demonstrations.

Keywords: DC and AC Josephson voltage standards, Josephson junction series arrays, junction stacks, power splitter, quantum voltmeter, impedance measurement, programmable Josephson voltage standards

(Some figures may appear in colour only in the online journal)

* Author to whom any correspondence should be addressed.

1. Introduction

Today, electrical quantum metrology is a very active field of research and development aiming for reliable and easy to use electrical quantum standards. The intrinsic high accuracy of quantum-based standards, combined with their automated operation, results in considerable benefits when short turnaround times for calibrations with the best possible uncertainties are required. Therefore, a large amount of research is being carried out on quantum current standards based on single electron pumps, resistance standards based on new materials for the quantum Hall effect, and Josephson voltage standards (JVSs) which are propagating towards AC applications. Even 60 years after the discovery of the Josephson effect, quantum voltage standards are still an active development subject to extend operating ranges towards higher voltages and frequencies. In addition, more compact and robust setups—ideally turnkey systems based on cryo-coolers—are being developed for a wider spread of systems in bringing quantum standards to calibration laboratories and industry. For voltage, these novel systems are based on either programmable JVS (PJVS) or pulse-driven JVS which we call Josephson arbitrary waveform synthesizer (JAWS). In the past ten years, cf (Behr *et al* 2012), progress has been achieved in fabricating large Josephson arrays, benefitting from improvements in fabrication technologies and microwave designs mostly for pulse-driven arrays. Many new Josephson-based applications were tested, some of them are developed into routine calibration procedures and instruments became commercially available.

The basic principle of PJVS is that the combination of a DC and a high frequency (HF) current f drives N flux quanta Φ_0 through the M junctions of an array. The Josephson constant $K_J = 2e/h$ with the Planck constant h and elementary charge e is the inverse of the flux quanta Φ_0. After the redefinition of the Système International d'Unités (SI) (BIPM 2019) in May 2019 JVS have become direct realizations of the volt. As a single flux-quanta transfer delivers only a very small voltage $\Phi_0 \approx 2$ μV GHz^{-1} many Josephson junctions (JJs) implemented in a series array are necessary to achieve practicable large output voltages. For our PJVS and JAWS arrays SNS-type JJs are used (S…superconductor, N…normal conductor). SNS junctions provide non-hysteric current–voltage characteristics without and with microwave irradiation. A detailed description for the fabrication of large PJVS arrays is given in (Yamamori *et al* 2006, Mueller *et al* 2007, 2009, Dresselhaus *et al* 2011, Behr *et al* 2012, Müller *et al* 2014). PJVS arrays are divided into segments or subarrays and computer controlled bias sources for the individual segments enable 'programming' the output voltage across the Josephson array. Synthesis of AC waveforms with PJVS was proposed by Hamilton *et al* (1995). Possible ways and limitations of AC waveform synthesis with PJVS were discussed in detail in (Behr *et al* 2012).

The JAWS operates JJs with current pulses of short duration, as introduced by (Benz *et al* 1996). In pulse-mode operation the Shapiro steps are selected by adjustment of the pulse amplitude (see figure 1). Large Shapiro steps are generated for all pulse repetition frequencies below the characteristic frequency f_c of the SNS junctions (Benz *et al* 1996). Furthermore, a broadband microwave circuit design is an important precondition for operating the JAWS properly. Depending on the polarity of the current pulses repeating with frequency $f_p(t)$, the voltage across a series array with M JJs follows $V(t) = \pm N \cdot M \cdot \Phi_0 \cdot f_p(t)$ when each pulse transfers N flux quanta Φ_0. The Josephson array is employed as a three-level (as we use $N = +1/0/-1$) quantum accurate quantizer in a sigma-delta digital to analog converter. Typically, the modulator frequency corresponds to the characteristic frequency of the JJs, about 15 GHz, and provides oversampling ratios larger than 1 million for signal frequencies of typically 1 kHz usually applied for high accuracy ac measurements at National Metrology Institutes (NMIs). On-chip filters exploit superconducting inductances to filter quantization noise at the output used for metrological purposes. Commercial pulse pattern generators (PPGs) are used to store the pattern of positive and negative current pulses that generate the desired waveform across the M JJs in the series array.

In this paper we summarize the main contributions that the Physikalisch-Technische Bundesanstalt (PTB) has made to the development and deployment of Josephson arrays in metrology in the past ten years. To underpin that the field of electrical quantum voltage metrology is still propagating towards AC applications we included new results and analyses in all sections. The contributions from other research or metrology groups are covered in additional papers in this special journal feature. Section 2 provides an update of ongoing developments in fabrication technology to further increase the output voltage of pulse driven series arrays to reach amplitudes higher than 1 V (Benz 2015a, 2015b, Kieler *et al* 2015) or even 4 V (Flowers-Jacobs *et al* 2019). Present research areas are stacking of JJs and parallelization by microwave power splitters or optical drives. Section 3 the 'Josephson voltage standard toolbox and their application fields' illustrates application areas and achievable uncertainties. Section 4 concentrates on JVS that are used as a measurement standard in calibrations. Josephson systems that are the basis for synthesizer applications are discussed in section 5. Conclusions and an outlook follow in section 6.

2. Progress in the fabrication of JJ series arrays

As already mentioned above many NMIs succeeded in fabricating 10 V PJVS arrays (Yamamori *et al* 2006, Müller *et al* 2007, Mueller *et al* 2009, Dresselhaus *et al* 2011, Behr *et al* 2012, Müller *et al* 2014). PTB also successfully demonstrated 20 V PJVS arrays (Müller *et al* 2013) already in 2013 and concentrated on fabrication of JAWS arrays after having demonstrated a good fabrication yield with suitable microwave design for 10 V PJVS arrays (Müller *et al* 2014). In this section we focus on the fabrication technology of JAWS arrays.

2.1. JAWS circuit design

The high-speed pulse-drive of the JJ arrays requires an appropriate RF circuit design which ensures both low microwave

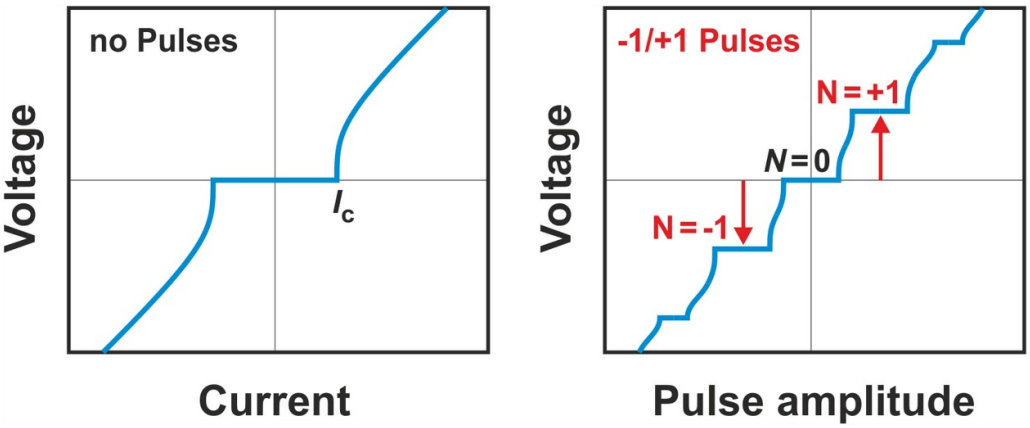

Figure 1. Schematic current–voltage characteristic of SNS junctions without and with pulse irradiation.

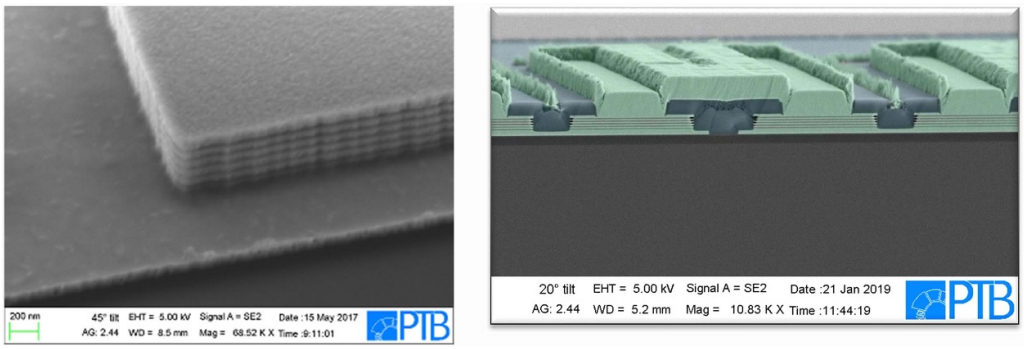

Figure 2. SEM images of Josephson junctions: (a) five-JJ stack after two fabrication steps and (b) cross-section of JAWS series array with five-stacked JJ after complete fabrication.

damping and low pulse dispersion. Therefore, the JJs are embedded in the center line of a broadband coplanar waveguide (CPW). The CPW impedance is tapered from 50 Ω to 37 Ω to compensate for the junction attenuation along the line and terminated by an on-chip thin film resistor (37 Ω). Low-pass LCR-filters (Watanabe *et al* 2006) at the voltage output and bias current input leads are integrated in thin film technology. They prevent the transmission of the input pulses along these lines, which would create distortions in the synthesized waveforms. The standard JAWS chip layout contains two independent JAWS arrays which are typically connected on-chip for summing up the voltage. Further methods to increase the output voltage are discussed in the next sections.

2.2. Stacked JJs

The fabrication of the JAWS circuits is performed in the PTB clean room facility (class ISO 5). SNS JJs with Nb_xSi_{1-x} as the normal-metal barrier material are used (Baek *et al* 2006, Kieler *et al* 2013a). Junction properties like critical current I_c and critical voltage V_c are adjusted nearly independently by choosing the composition x and the thickness of the barrier d. Typical JJ parameter are $I_c \approx 3$–5 mA and a normal resistance R_n of about 3 mΩ. However, the JJ operation frequency can be tuned from about 1 GHz to 150 GHz (and beyond).

An advantage of these SNS-type junctions is that they can be deposited and patterned in stacks, which offers the benefit to increase the integration density of the JAWS circuits (Flower-Jacobs *et al* 2020). In this way the CPW can be shorter for the same number of JJs improving pulse dispersion and, in addition, coupling between the junctions is stronger. A sophisticated 'window type' process for the fabrication of up to 5-stacked JJ arrays was developed at PTB (Kieler *et al* 2021). The thicknesses of resist as well as of the Nb and SiO_2 layers were increased. Additionally, the SiO_2 is deposited by plasma-enhanced chemical vapor (PECVD) and atomic layer deposition (ALD). A thin ALD layer right before the PECVD process ensures a perfect edge coverage of the tall junction stacks. Chemical mechanical polishing of the SiO_2 layer was introduced to guarantee a smoother surface before deposition of the Nb-wiring layers. More details about our process can be found in (Kieler *et al* 2015, 2021). Figure 2 shows a side view of the five-junction stack after two fabrication steps (left) and a cross-section of a JAWS array with five-stacked JJs after complete fabrication (right). By analyzing the data of about 300 JAWS arrays with a total junction count of more than 2 million a high junction yield of 99.99% was derived. This is sufficient for our level of circuit integration density and number of fabricated wafers.

There is a high impact of realizing this five-stacked junction technology, as we can synthesize an effective output voltage

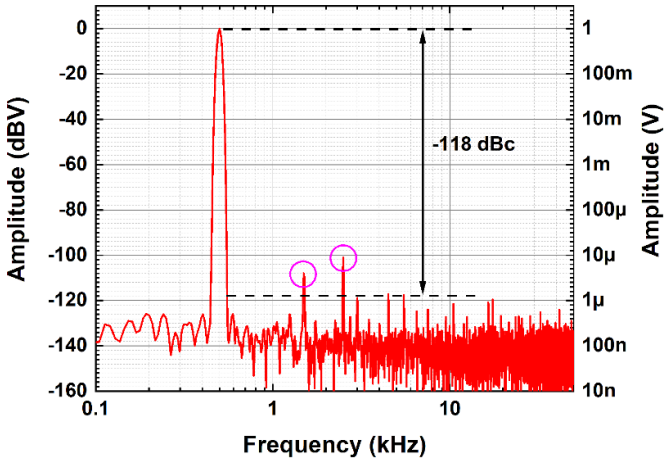

Figure 3. Frequency spectrum of a 1 V_{rms} sine wave at 500 Hz synthesized with two chips and 60 000 junctions. Harmonics are suppressed by −118 dBc. The circles **O** indicate harmonics which appear due to the limited linearity of the sampler (Benz *et al* 2015a).

of 1 V with series operation of 4 arrays integrated on 2 chips. This is an improvement to our first realization of 1 V_{rms} with 8 arrays on 4 chips (Kieler *et al* 2015). A spectrum of a sine wave generated with 60 000 junctions at 500 Hz is shown in figure 3. Higher harmonics are suppressed by at least 118 dBc which is the specification of the digitizer used to measure the spectrum (NI, Benz *et al* 2015a). In 2017 (Kieler *et al* 2017) we were able to operate 16 arrays in series with a total number of 162 000 junctions to achieve an output voltage of 2.25 V. Finally, an important goal would be to achieve 7 V_{rms} with a compact JAWS. Such a system would be the ultimate Josephson voltage standard. The U.S. National Institute of Standards and Technology (NIST) already demonstrated successfully compact 1 V_{rms} JAWS and even an output voltage of 4 V_{rms} by combining two systems (Flowers-Jacobs *et al* 2016b, Benz *et al* 2015a, Benz *et al* 2015b, Flowers-Jacobs *et al* 2019). More compact systems with less RF inputs are possible with on-chip power dividers which will be discussed in the next section.

To evaluate the JAWS arrays the chips are mounted on special designed carrier boards (typical material Rogers 3006) and are electrically connected by Al wire bonding. The carrier boards contain 50 Ω CPW's with microwave launcher used to mount the JAWS chips into cryoprobes. The chips are shielded by magnetic cryoperm screens and cooled to 4 K either in liquid helium dewars or pulse-tube cryocoolers. At PTB, we are usually using high-speed ternary PPGs (Sympuls BPG30G[1]) delivering −1/0/+1 pulses with a maximum clock frequency of 15 GHz and a 512 Mbit pulse code memory. By means of a higher-order sigma-delta modulation (Kieler *et al* 2009) the desired waveform is digitized into such a bit pattern and transferred to the PPG memory. For the AC coupling operation mode (Benz *et al* 2001) arbitrary waveform generators deliver the compensation signals to each array while the output waveforms are analyzed by a commercial fast digitizer (NI, Benz *et al* 2015a).

[1] Identification of commercial equipment does not imply an endorsement by PTB or that it is the best available for the purpose.

2.3. On-chip power dividers

To simplify the existing JAWS set-up at PTB and to increase the amplitude of the synthesized AC voltages generated by one PPG channel and by using series operation of several JAWS arrays, on-chip broadband RF power dividers were developed and successfully integrated with JJ series arrays. The RF power dividers are passive electrical components, which are used for power dividing and power combining. They usually have one input port and several output ports. In our case, these dividers were used to divide one RF pulse input signal from PPG into two or four RF pulse signals, so that multiple parallel JJ arrays were operated by less PPG channels and connected with each other to enable spectrally pure waveforms to be synthesized.

Recently, two main types of on-chip power dividers with the equal division were investigated. They are serial-parallel power dividers and Wilkinson type power dividers. PTB's serial-parallel power divider is based on the equivalent circuit model of (Yamamori and Kohjiro 2016) for the PJVS at the Japanese National Institute of Advanced Industrial Science and Technology. It has been successfully implemented into the JAWS circuits at PTB (Tian *et al* 2020, 2021). Instead of using lumped elements like NIST does (Elsbury *et al* 2009), our Wilkinson type power dividers include ¼ λ resonators and the coplanar stripline (CPS) bending structure. Among these Wilkinson power dividers, three variations of designs were developed: one-stage single-section Wilkinson dividers (Tian *et al* 2020), one-stage three-section Wilkinson dividers and two-stage single-section Wilkinson dividers (Tian *et al* 2021). 3D models of the power dividers were simulated with CST Microwave Studio[1]. In the simulation set-up, the frequency range was set to 0–30 GHz which amply covers our typical PPG pulse repetition frequency of 15 GHz. The normal background and magnetic boundaries were used for modeling the on-chip power dividers, because the superconducting JAWS chip was mounted in a cryoperm shield in the measurement. The parameters and design material in the simulation were quite comparable to the actual fabrication process. The size of the on-chip power dividers is compact enough to be placed within a 10 mm × 15 mm chip. The S-parameter sweep was used to simulate and optimize the designed structure. Figure 4 presents one of the simulation results of our designs. The transmission coefficients of the two-stage serial-parallel power divider are close to the theoretical value of −6 dB. Its reflection coefficient is better than −20 dB. The curves of the transmission coefficients are very flat, as there is no frequency dependent component in this design.

The simulation show that all the designed power dividers have a broadband performance, which is very suitable for JAWS applications. The two-stage serial-parallel power divider is the most broadband and compact of all the designed power dividers. However, the insulation of the output ports is not guaranteed. And the phase balance of the output ports is 180°. All the Wilkinson type power dividers have a good

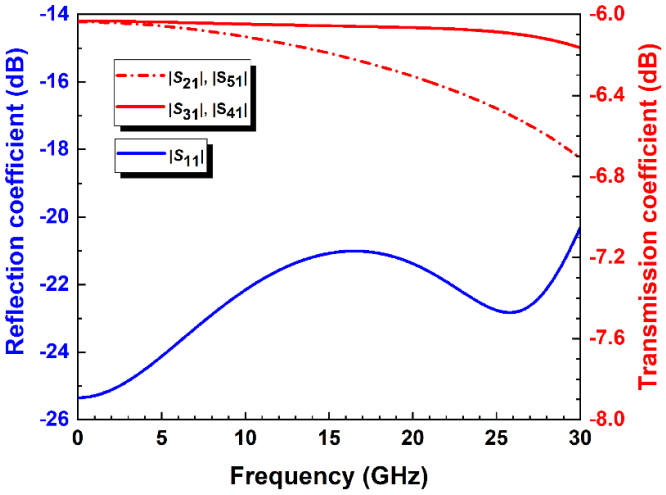

Figure 4. Numerically simulated transmission coefficients (red axis on the right) and reflection coefficient (blue axis on the left) of the serial-parallel power divider (Tian *et al* 2020).

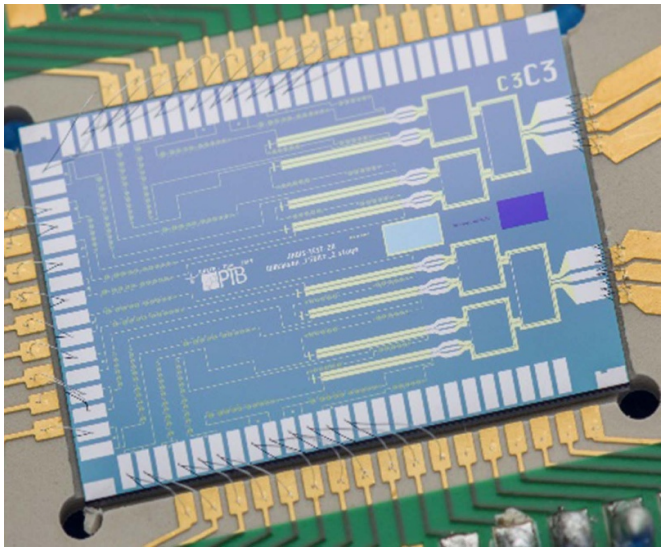

Figure 5. A photograph of the mounted microwave package with an integrated JAWS chip with two-stage Wilkinson power dividers. The chip was connected to the PCB carrier through bonding wires.

isolation and there is no phase shift in their outputs. Due to the CPS bending structure, they are still in a compact shape.

The tapered on-chip inner-outer DC-block capacitor (high pass filter) were integrated with the outputs of the power divider as well. Figure 5 shows a photograph of such a JAWS chip, which contains two identical integrated circuits with on-chip two-stage power dividers. The on-chip power dividers were also successfully integrated into the previous described fabrication process without involving additional process steps. The chip was connected to the PCB carrier through bond wires.

Figure 6 shows that an array with one-stage single-section Wilkinson power divider and 18 000 JJs (6000 triple-stacked JJs) was operated up to a clock frequency of 14 GHz (return-to-zero pulses) with 81.4% code amplitude. An AC output

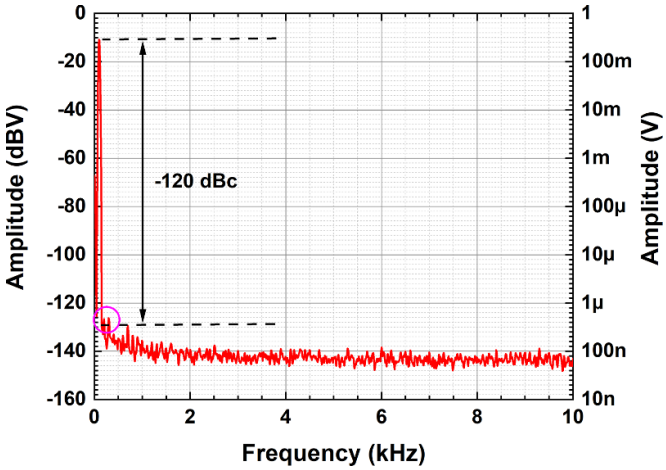

Figure 6. Frequency spectrum of a synthesized 100 Hz sine wave using a JAWS array with the one-stage single-section Wilkinson power divider and 18 000 Josephson junctions ($V = 300\ \mathrm{m}V_{\mathrm{rms}}$, $f_{\text{clock-PPG}} = 14$ GHz, $A_{\Sigma\Delta} = 0.814$). The circles **O** indicate harmonics which appear due to the limited linearity of the sampler (Benz *et al* 2015a).

voltage of 300 $\mathrm{m}V_{\mathrm{rms}}$ per RF channel is synthesized. No higher harmonics are visible above the noise floor. To further increase the amplitude of the synthesized AC voltages, both RF channels were used, and the arrays were connected by a superconducting wire resulting in 36 000 JJ operated simultaneously. A synthesized 600 $\mathrm{mV_{rms}}$ sine wave was generated by a single JAWS chip, however, due to crosstalk between the two arrays harmonics are increased by about 15 dB (Tian 2022). Work is ongoing to reduce crosstalk between arrays, RF and compensation lines.

So far, it has been experimentally demonstrated that the designed on-chip power dividers are quite broadband and successfully integrated with JAWS circuits. In the future, we plan to integrate larger series arrays together with on-chip power dividers to continue increasing the output voltage of a single chip containing several JAWS arrays.

2.4. Optical driven JAWS

Operation of Josephson arrays with opto-electronically transmitted pulses was already demonstrated in (Williams *et al* 2004) using 100 Josephson SINIS junctions. As part of a recent European research project, the operation of commercial InGaAs photodiodes (PDs) (Albis 2022) at 4 K was demonstrated together with a robust alignment method for the optical fiber and the PD (Bardalen *et al* 2017) as illustrated in figure 7. Shortly thereafter, pulses were used to drive SNS Josephson arrays with 3000 junctions (Karlsen *et al* 2019, Kieler *et al* 2019, Herick *et al* 2020). The PD is providing a 100 µm large lens making the implementation easy. The Si-carrier chip is glued, and Al wire bonded to a PCB. The JAWS- and PD-chip are connected by bonding. Detailed optimizations and investigations of the high-speed performance at room-temperature and 4 K were performed (Bardalen *et al* 2017, Bardalen 2018)

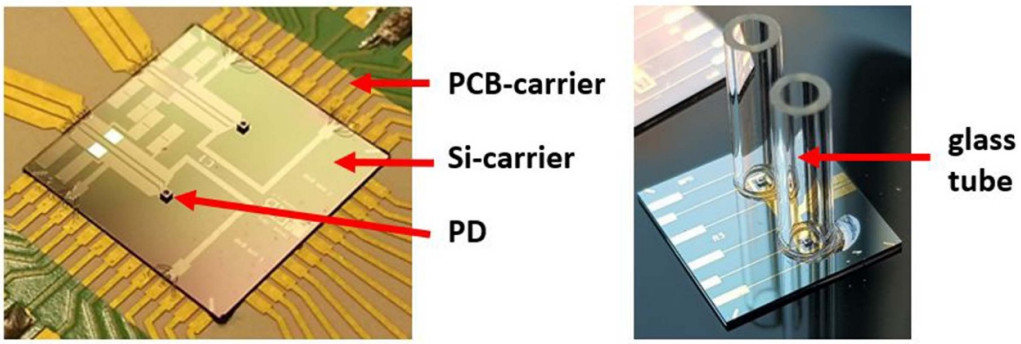

Figure 7. Photographs of two photodiodes (PDs) flip chip mounted to a Nb CPW manufactured on a Si chip at PTB (left) and a different Si-carrier chip mounted with two PDs, each one aligned to a glass tube for holding the ferrule ended glass fiber (right).

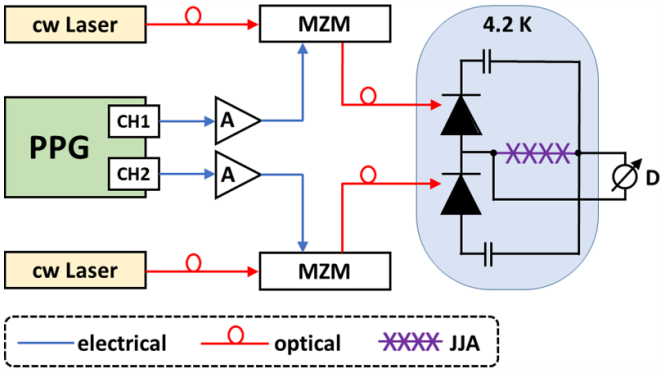

Figure 8. Schematic of the optical-driven JAWS for bipolar waveforms after (Herick *et al* 2020). Two separate channels are used, one for each polarity. Electrical PPG pulses are amplified (A) before for the modulation of the optical signals (laser light) with Mach–Zehnder Modulators (MZM). The MZM output signals are sent via fibers to two PDs ▲ which are mounted next to the JJ array (JJA). The output of the JJA is measured with a spectrum analyzer (D).

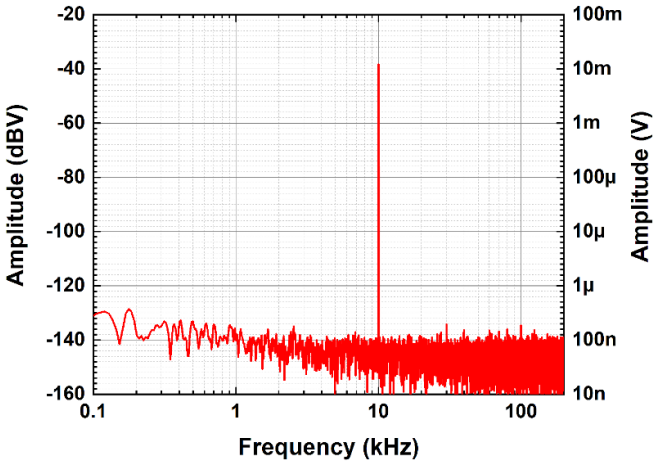

Figure 9. Spectrum of a 12.5 mV_{rms} sine wave at 10 kHz generated with the bipolar optical pulse setup shown in figure 8. A JAWS array with 3000 Josephson junctions was operated at 10 GHz clock frequency.

and the optical pulse setup is described in (Karlsen *et al* 2019).

The aim of the development is to enable a possible low-cost solution for parallel operation of many JAWS arrays by operating fast PDs at 4 K close to the JAWS arrays. Furthermore, operating JJ with PDs does not require the AC coupling technique. Without all these electrical lines in the cryoprobe and by using optical fibers instead of semi-rigid cables crosstalk will be significantly reduced, especially at signal frequencies above 10 kHz.

Figure 8 shows a simplified optical-driven JAWS setup for bipolar waveforms (Herick *et al* 2020). The pulse pattern is provided by two PPG channels and electrically amplified by the RF modulator driver (A). The amplified pulses are transferred electrically to the Mach–Zehnder modulators (MZM) which modulate the light of two 1310 nm Fabry–Perot lasers according to the pulse pattern. The optical fiber transfers the light pulses to the high-speed (28 Gbit s^{-1}) InGaAs PDs at 4 K.

Using a one-channel optical pulse-drive, unipolar sine waves were synthesized with stable operation margins using a 3000 junctions JAWS array in a signal frequency range from 60 Hz up to 10 kHz. With clock frequencies up to 15 GHz 6.6 mV_{rms} voltage were generated (Kieler *et al* 2019). Following to this, a two-channel optical pulse-drive setup for generation of bipolar waveforms was established at PTB (figure 8). First spectrally pure bipolar waveforms were synthesized with the same JAWS array operated at 10 GHz with 100 µA-margins. Figure 9 shows a spectrum of a 12.5 mV_{rms} sine wave at 10 kHz where higher harmonics are suppressed by more than 95 dBc (Herick *et al* 2020).

Many further papers on implementation techniques, measurement setups, investigations and waveform synthesis (Ireland *et al* 2017, 2019, Bardalen *et al* 2020, Karlsen *et al* 2020, Nissilä *et al* 2021, Brevik *et al* 2022) indicate that the optical drive is a very active field with high potential for applications.

3. The Josephson voltage standard toolbox and their applications fields

3.1. Systems and application areas

As has been already mentioned two different types of JVS for AC applications are developed. On the one hand the pulse-driven Josephson standard (JAWS) and on the other hand PJVS. The constraints of the RF design in the transmission lines are less strong with continuous microwave compared to the constraints imposed by the broadband nature of the pulse drive. This, in turn, has an impact on the number of JJ that can be irradiated with the same power and consequently on the output voltage that can be reached. Due to the much simpler operation with continuous microwaves PJVS with arrays up to 20 V were developed (Müller *et al* 2013). Presently, the highest JAWS voltage of 4 V_{rms} was reported by NIST (Flowers-Jacobs *et al* 2019). With JAWS, AC voltages are synthesized by fast flux quanta transfer on a picosecond time scale at 15 GHz clock frequency. At much lower frequencies e.g. up to 1 MHz, spectral pure waveforms can be generated, making JAWS a perfect voltage signal synthesizer (figure 10(a)), whereas a spectrum of a PJVS-generated waveform has many harmonics. These harmonics are caused by the limited number of segments in binary divided Josephson arrays (figure 10(b)). A synthesis of metrological meaningful sine waves is additionally limited due to unpredictable transients. However, the relative simplicity of fabricating 10 V PJVS and the combination with sampling procedures lead to a robust, highly accurate measurement system called 'AC quantum voltmeter' (AC-QVM) (Behr *et al* 2007).

In the following we will look at metrological applications which have been tackled by either JAWS or PJVS. The variety of Josephson systems can be viewed as a toolbox. Each system has a specific strength which is an advantage for a certain application. Figure 11 summarizes such applications in electrical metrology which span a parameter space from DC to up to 1 MHz in frequency range and from mV to 10 V voltage regarding signal amplitudes.

Conventional DC JVS based on superconductor-insulator-superconductor (SIS) arrays are gradually replaced in NMIs worldwide by PJVS systems which have been proven robust and reliable. In addition to classical metrological DC voltage, applications like calibration of Zener references and linearity measurements on digital voltmeter, JVS are increasingly deployed as very stable and traceable references.

An easy extension turns such PJVS to AC-QVM which are suitable for AC voltage calibrations up to the kHz range (Lee *et al* 2013). Recently, the frequency range of the AC-QVM has been extended up to 100 kHz (Behr and Palafox 2021). Due to the reliability of the AC-QVM, systems were commercialized (Schubert *et al* 2015) and methods were expanded for calibrating DC and AC currents and resistances (Lee *et al* 2016).

Primarily, due to the lack of JAWS with amplitudes above 10 mV, Josephson impedance bridges were developed based on PJVS (Lee *et al* 2010). For similar impedances, PJVS based bridges should synthesize square waves to limit the influence

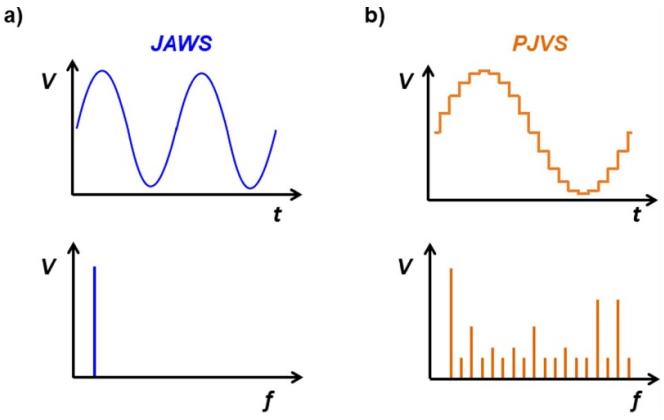

Figure 10. Schematic comparison of a JAWS sine wave *versus* PJVS stepwise approximated sine wave. The upper curves display time traces and the lower ones the associated spectra. Higher harmonics in the spectrum of the stepwise approximated sine wave appear due to the limited resolution in binary divided Josephson arrays.

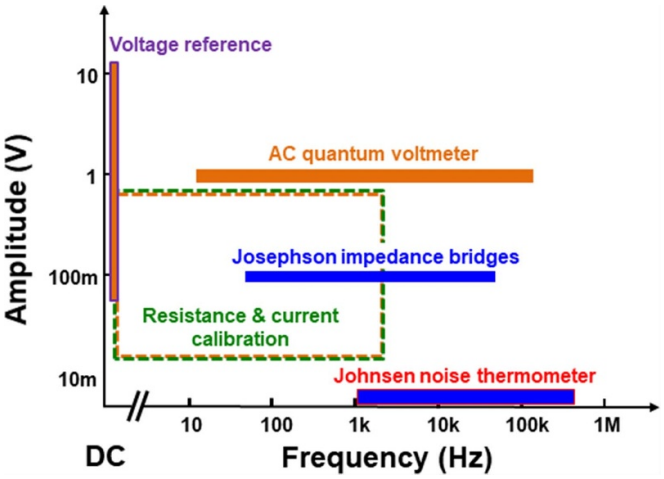

Figure 11. Josephson-based applications cover the frequency range from DC to 500 kHz and voltage amplitudes from a few mV to 10 V. These applications are discussed in the next sections.

of transients. Higher harmonics cancel almost perfectly, and very accurate 1:1 and 10:1 ratio calibration of the order of 10^{-8} are possible by using such PJVS bridges (Hagen *et al* 2017), however, they are limited to relative uncertainties of few parts in 10^6 for quadrature measurements (Palafox *et al* 2012). Especially such quadrature calibrations are gaining importance with the advent of new and user-friendly QHR standards based on materials such as graphene. Beside all the advantages of a quantum based and, hence, stable output amplitude with very low noise, JAWS is an ideal source for Josephson impedance bridges (Overney *et al* 2016, Bauer *et al* 2017) and for calibrating AC devices like inductive voltage dividers (IVDs) (Herick *et al* 2018). Furthermore, JAWS can be utilized for the precise and spectrally pure generation of waveforms (Benz *et al* 2000, Palafox *et al* 2018), and it is an ideal candidate for Johnson noise thermometry (Nam *et al* 2003, Benz *et al* 2011, Kraus *et al* 2021, Drung *et al* 2022). In addition, also a phase angle

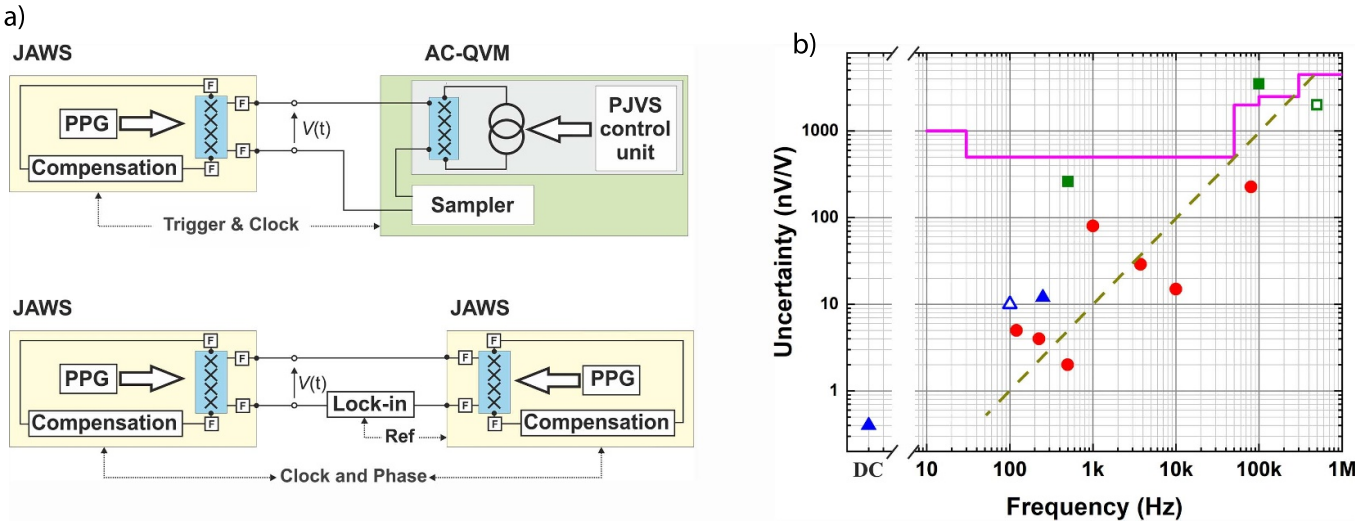

Figure 12. (a) Schematics for direct JAWS *versus* PJVS and JAWS *versus* JAWS comparisons. (b) The pink line ▬ shows PTB's CMCs for AC-DC transfer ($k = 1$) as reference. Uncertainties for Josephson AC voltage comparisons also via IVDs and impedance bridges are marked with dots accordingly ● JAWS *versus* JAWS (Kieler *et al* 2013b, Flowers-Jacobs *et al* 2016a, Herick *et al* 2018, Overney *et al* 2020) ▲ AC-QVM *versus* JAWS (Jeanneret *et al* 2011, Behr *et al* 2015, Rüfenacht *et al* 2018, Kraus *et al* 2020) ■ different indirect comparisons via or with conventional standards (Jeanneret *et al* 2011, Bauer *et al* 2021). Open symbols (**Δ,** □) are only valid for type-A uncertainty (Rüfenacht *et al* 2016, Kraus *et al* 2020). The dotted line shows a linear increase with frequency.

standard can be realized in different ways, where two possibilities are already in used and published. The first solution uses a single JAWS array to generate a fundamental tone and corresponding harmonics with desired phase relations with respect to the fundamental (Georgakopoulos *et al* 2019). Another solution is to generate signals with a desired phase angle from two JAWS systems (sine waves of the same frequency) by adding a well-known delay between both signals (Bauer *et al* 2020b, Bauer *et al* 2023). This is done by a PPG with two independent but synchronized memories with a resolution of 250 fs.

Before we give more insight into these applications in the sections 4 and 5, we need to clarify which uncertainty levels we could expect from Josephson-based systems at different frequencies.

3.2. *Verification by comparisons*

Verification of standards is one of the main tasks in metrology, and newly developed quantum standards require a detailed uncertainty review. In many cases such verification turns out to be difficult as no conventional standards of similar quality in the sense of accuracy performance are available. For AC voltage metrology, thermal transfer standards have been well developed and cover the frequency range from 10 Hz to 10 MHz. In the audio range, relative uncertainties at a level of parts in 10^7 are commonly achieved. Towards higher frequencies, the uncertainties are typically increasing very slowly. During calibration, thermal transfer standards are connected next to each other and hence do not suffer from long cables which is the case for JVS.

To verify JAWS and PJVS at a better uncertainty level than 10^{-7}, direct comparisons must be performed. Such comparisons are established for DC and many of them were carried out (BIPM KCDB). For AC voltage, direct comparisons were carried out between two JAWS (Kieler *et al* 2013b) and between a JAWS and AC-QVM (Behr *et al* 2015). Figure 12(a) shows schematic setups of the JAWS *versus* PJVS and JAWS *versus* JAWS comparisons. Direct Josephson AC voltage comparison are more complex compared to DC comparisons. Beside common problems with ground loops and interferences, also, e.g. the phase between the standard-generated signals, cable corrections, effects of on-chip inductances, and the bandwidth of the null-detector must be considered. To avoid some of these problems, indirect comparisons have been performed with good results (Jeanneret *et al* 2011). Figure 12(b) displays AC voltage comparison with PJVS and JAWS in the frequency range up to 500 kHz (data points). The dashed line, as guide to the eye, demonstrates that the uncertainty for AC Josephson voltage comparisons follow roughly a linear increase starting with 10^{-9} (relative uncertainty) at 100 Hz. The solid pink line represents a typical uncertainty benchmark for AC-DC transfer measurements with thermal converters. Below 50 kHz, lower uncertainties are achieved with Josephson-based AC voltage standards.

The next sections will discuss Josephson comparisons in more detail.

3.2.1. JAWS versus PJVS (DC). A first DC comparison of a JAWS and a PJVS was performed by NIST (Rüfenacht *et al* 2016, 2018). Here we report on a similar comparison that was carried out at PTB at the 1 V level. About 80 measurements in a $+--+$ —sequence were performed automatically within 90 min. 160 $+-$ —data are averaged and displayed in figure 13(a). Even though four outliers are visible—probably the 4 s waiting time after reversal of both quantum standards was chosen slightly too short—the relative agreement of 3×10^{-10} with a type-A uncertainty of 4×10^{-10}, evaluated

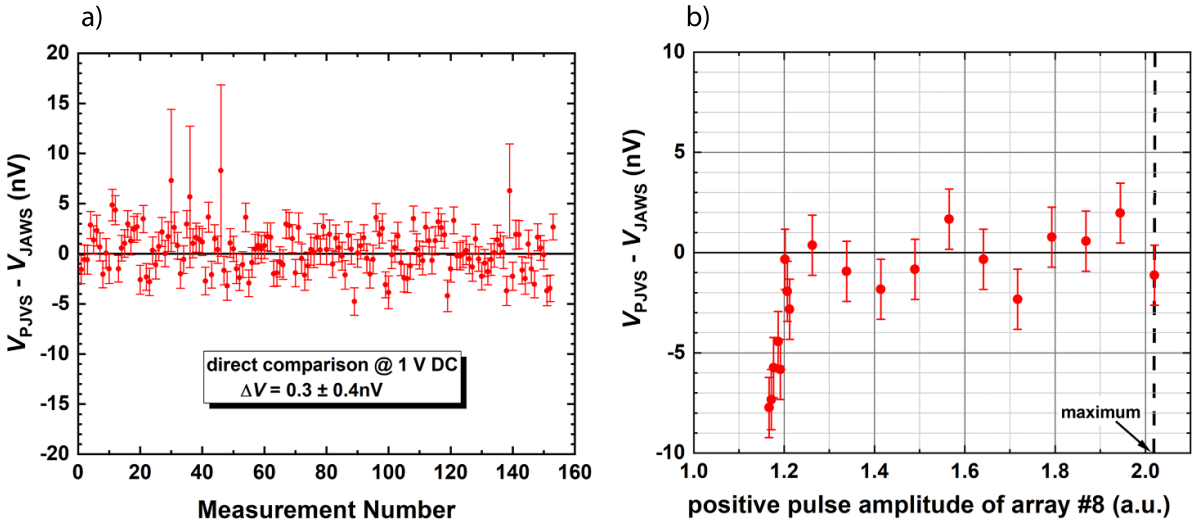

Figure 13. (a) Automated 90 min direct comparison of a JAWS and PJVS at 1 V level. (b) QLR for the positive pulse amplitude of array number 8.

by an Allan deviation analysis, is within expectation. Systematic errors like leakage, frequency offset, etc were analyzed and are much smaller than the dominating type-A uncertainty. This conclusion is underpinned by parameter sweeps demonstrating quantum margins or a quantum locking range (QLR). An example for a pulse amplitude sweep is shown in figure 13(b).

3.2.2. JAWS versus PJVS (AC). An indirect comparison between a PJVS and a JAWS using an ADC as transfer device was performed at 100 mV level and 500 Hz showed a good agreement with a relative voltage difference of $(-1.8 \pm 2.6) \times 10^{-7}$ ($k = 2$) (Jeanneret *et al* 2011). The first direct PJVS *versus* JAWS comparison (Behr *et al* 2015) was carried to evaluate the uncertainty of PTB's 1 V JAWS and, at the same time, the AC-QVM. On the one hand, PTB's 1 V JAWS consists of a series connection of eight arrays which are all operated in the so-called AC-coupling mode (Benz *et al* 2001). Therefore, the setup requires combining eight high-frequency pulse codes each one compensated by a low-frequency current. On the other hand, the AC-QVM was further developed and has become a commercially available product (Supracon AG). So far, however, it was only used to calibrate conventional standards with limited uncertainty (Rufenacht *et al* 2009, Kim *et al* 2010, Williams *et al* 2011, Lee *et al* 2013, Rüfenacht *et al* 2013).

The very good agreement $(0.35 \pm 1.2) \times 10^{-8}$ ($k = 1$) of both quantum standards impressively demonstrated two things. The AC-QVM is suitable for calibrations at the level of 10^{-8}, an uncertainty improvement of more than one order in magnitude, and it is possible to combine many pulse-driven Josephson arrays in a complex setup.

3.2.3. JAWS versus JAWS (AC). Besides JAWS *versus* PJVS comparisons, it is also possible to compare two JAWS to investigate their accuracies mutually. In the past, this has been performed by connecting two JAWS arrays in series and applying a 180° phase shift between both sinusoidal waveforms and by measuring the residual, differential voltage with a lock-in amplifier as null detector. The documented results of the relative difference of 1.6 parts in 10^8 at a signal frequency of 3.75 kHz (Kieler *et al* 2013b, Rüfenacht *et al* 2016) and of 8 parts in 10^8 at 1 kHz (Flowers-Jacobs *et al* 2016a) showed a very good agreement between the two JAWS. A repetition of the experiment proposed in (Kieler *et al* 2013a) at different signal frequencies also showed an agreement within 0.2 parts in 10^7 up to 10 kHz (Kraus *et al* 2018). Further applications like IVD calibration (Herick *et al* 2018) (see section 5.3) and the development of Josephson impedance bridges based on JAWS (Bauer *et al* 2017, Overney *et al* 2020) (see section 5.4) as well rely on these properties. Therefore, these experiments are also recorded in figure 12(b). However, here it is important to mention that the uncertainties in these experiments are surely influenced by the specific setups and additional components even though, e.g. cable and inductive errors partly cancel out in an impedance bridge (Overney 2018).

Above 10 kHz, however, significant deviations were found that indicate systematic errors in pulse-driven Josephson systems (Kraus *et al* 2018). This is in line with past experiments investigating these deviations on different development sites (Burroughs *et al* 2003, Landim *et al* 2008, Kieler *et al* 2008, Filipski *et al* 2008, van den Brom *et al* 2016, Zhao *et al* 2017). Recent developments introduce new pulse-bias techniques (Benz and Waltman 2014, Zhou *et al* 2015, Brevik *et al* 2017) to further mitigate high-frequency voltage errors in the JAWS. The understanding and mitigating of these errors are major tasks, especially in high-frequency applications of pulse-driven Josephson arrays, to ensure the accuracy of the synthesized AC voltage. Therefore, an indirect comparison between two JAWS has been carried out for signal frequencies up to 500 kHz (Kraus *et al* 2020). Each system produces a sinusoidal voltage with a nominal rms amplitude of $V_{\mathrm{rms}} = 10$ mV and are alternately connected to an

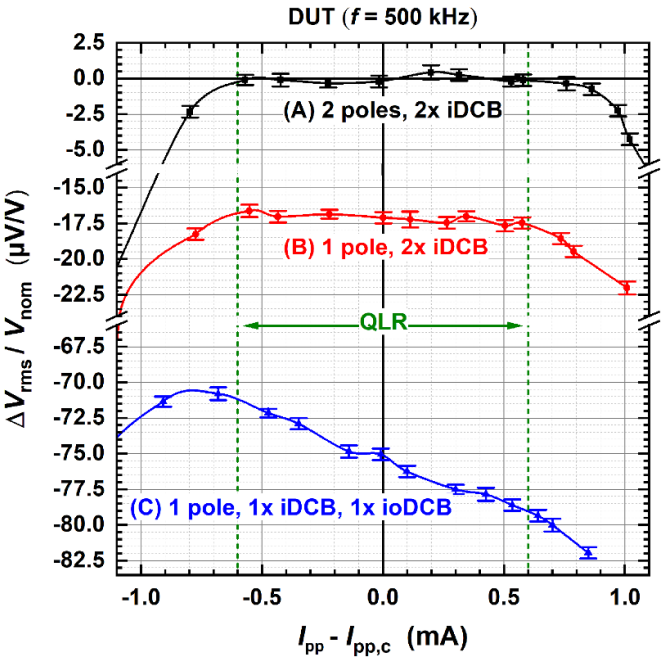

Figure 14. Relative deviation over the quantum locking range (QLR, green dashed lines at ± 0.6 mA) of the DUT JAWS at 500 kHz for the bias configurations A, B and C. $I_{\mathrm{pp,c}}$ denotes the pulse-bias amplitude setting when the DUT is centered on its QLR. In configuration A, in contrast to configuration B and C, a 3 dB attenuator is used between the two inner DC blocking capacitors (iDCB) forming a two-pole instead of a one-pole high-pass filter for the pulse-bias current. In configuration C the second iDCB is replaced with an inner-outer DCB (ioDCB) compared to configuration B. The solid spline curves are used to guide the reader's eye. The error bars indicate the type-A uncertainties ($k = 1$). Reproduced from (Kraus *et al* 2020).

analog-to-digital converter (ADC), which serves as a transfer standard. One system acts as a reference (REF), which remains unchanged during measurements and the other as the device under test (DUT). The deviation of both systems $\Delta V_{\mathrm{rms}} = V_{\mathrm{DUT}} - V_{\mathrm{REF}}$ is deduced from the measure amplitude spectra. In addition to the influence of the output cabling on the signal amplitude, which is well known in the literature and scales in first order quadratically with cable length and frequency (Zhao *et al* 2017, Underwood 2018), the influence of the pulse-bias current was investigated in detail.

The pulse-bias current consists of a low frequency component inherent in the HF pulse train. The low-frequency (LF) current is determined by the desired waveform, resulting in a current component at the signal frequency (Burroughs *et al* 2003, Landim *et al* 2008). Typically, DC blocking capacitors in the microwave setup of the JAWS are used to filter out this LF current. However, any remaining unfiltered part, denoted feed through current, is still transmitted to the JJ array and produces unwanted voltage signals at the signal frequencies. The resulting amplitude error, referred to as the feed through error, was measured and analyzed for three different high pass filtering configurations of the DUT (A, B, C) by varying the pulse-bias amplitudes I_{pp} at 500 kHz. The results are shown in figure 14. Note, that the amplitude error due to the output cabling is suppressed in the relative deviation between the two JAWS, as the cable lengths of both systems are precisely matched. For configuration A in figure 14, we see that the relative deviation between the DUT and REF JAWS stays within ± 1 μV/V for I_{pp}—$I_{\mathrm{pp,c}} = \pm 0.6$ mA. Varying I_{pp} over the QLR does not noticeably affect the relative deviation between both JAWS, indicating that the feed through error is sufficiently suppressed. Configuration B and C show clear dependencies, i.e. the DUT's signal amplitude is dependent on the bias-parameters even when operated on its QLR. The created model described in detail in (Kraus *et al* 2020) for the feed through error fits well with the experimental results and additional measurements. It is shown that less efficient filtering of the feed through current and/or an outer DCB in conjunction with parasitic inductances in the low-side of the output cabling result in large high-frequency voltage errors. The results of these ongoing investigations will improve the understanding of dominant high-frequency error mechanisms in the JAWS, essential for high-frequency applications of the JAWS, e.g. as a reference noise source in Johnson noise thermometry (cf section 5.5).

4. JVS as measurement system

Nowadays, Josephson voltage standard measurement systems are usually based on PJVS. PJVS voltage amplitudes of 20 V were achieved and due to continuous microwave operation, these systems are simpler and cheaper than JAWS. Thus, applications discussed in this chapter are always based on PJVS. However, a JAWS measurement system was already introduced (Flowers-Jacobs *et al* 2020). It is to be expected that such systems will occur more frequently once JAWS have achieved higher output voltages.

4.1. The AC quantum voltmeter

The basic functionality of the AC quantum voltmeter was already described in our last overview paper (Behr *et al* 2012). Since then, several NMIs developed improved AC-QVM (Lee *et al* 2013, Rüfenacht *et al* 2013, Amagai *et al* 2018, Kim *et al* 2020). Depending on the PJVS array and its bias source—called PJVS control unit in figure 12—and on the speed of the sampler, an AC-QVM covers voltages up to 10 V and frequencies up to a few kHz (see figure 15(c)). An AC voltage is calibrated by generating a waveform based on quantized voltage steps from a PJVS, synchronized to it and reconstructed from the measured differences of a sampler and the associated Josephson voltage steps. Figure 15(a) shows a schematic of stepwise approximation to a sine wave. The grey shaded areas indicate times when the difference between the sine wave (red curve) and Josephson waveform (blue curve) is being sampled. Due to its very good accuracy (see section 3.2.2) and the ability to achieve 10^{-8}-resolution within minutes, fully automated setups are commercially available (Schubert *et al* 2015). The superior ability to achieve very good uncertainties will lead in long-term to a replacement of thermal transfer standards as primary standards at NMIs. Thermal converters

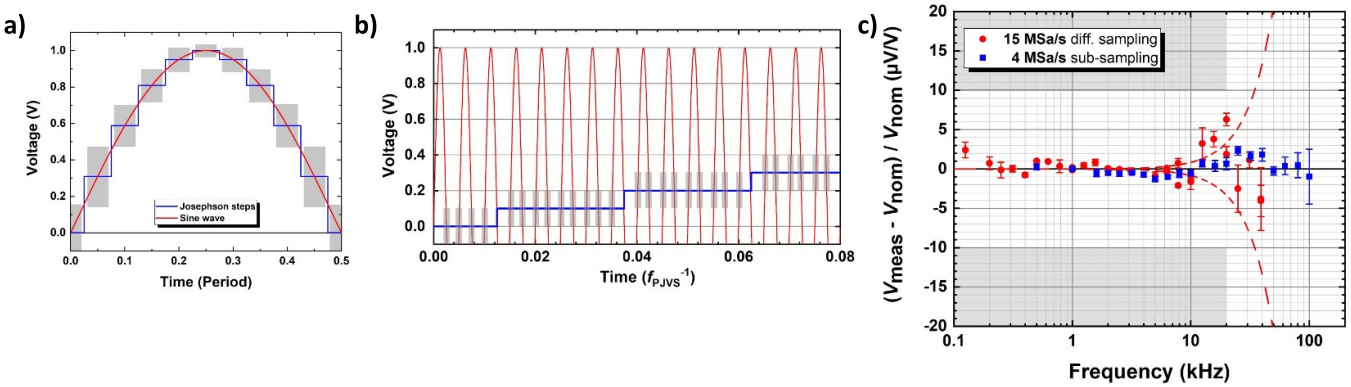

Figure 15. (a) Direct differential and (b) sub-sampling measurement schemes. The sine wave curves under test (red) are calibrated with Josephson stepwise curves (blue). (c) Results of differential sampling (●) and sub-sampling (■) up to 100 kHz at 1 V for the voltage difference V_{meas} and the nominal value of a Fluke 5700A calibrator[1] V_{nom}. A NI PXI 59221 was used to measure the voltage differences with sampling rates of 4 MSa s^{-1} and 15 MSa s^{-1}. The dashed line marks the uncertainty increase of differential sampling with increasing frequency. The error bars indicate type-A uncertainties ($k = 1$). The grey area marks the specification of the 5700 A.

require time-consuming measurements, but they are small, cheap and can be easily transported. For a complete move towards sampling techniques, improved AC voltage transfer standards are needed. Recently, improved sources were developed e.g. (Nissila *et al* 2016) and (Kučera *et al* 2020).

Direct differential sampling with the AC quantum voltmeter is limited in frequency to the kHz-range (figure 15(c)) because of the transients from the PJVS and limitations from the sampler. To overcome this limitation, a sub-sampling technique was developed which is described in the next section.

4.1.1. Sub-sampling up to 100 kHz. Figure 15(b) depicts the sub-sampling scheme following the idea of (Kürten Ihlenfeld and Landim 2016). During time intervals shown as grey zones, the voltage difference between the sine wave under test and Josephson voltage steps of a PJVS are sampled. Re-combining the HF sine wave (based on Josephson voltage steps) and measurements is feasible due to perfect synchronization (Bauer *et al* 2021). Even though much less data are taken during of each HF period in comparison with differential sampling, type-A uncertainties <1 µV/V below 50 kHz and 3.5 µV/V at 100 kHz are possible for five measurement repetitions with a total measurement time of about 5 min, as shown in figure 15(c). The red and blue points indicate the difference in measurements of a Fluke calibrator[1] using the AC-QVM in differential and sub-sampling mode for a conventional calibration by a thermal transfer standard. The grey zones show the $k = 1$ uncertainty for a calibrator used as transfer standard. It is obvious that the agreement is much better. The type-A uncertainty of the red differential sampling data increases above 10 kHz even when using a high sampling rate of 15 MSa s^{-1}. The transients in interaction with the finite impulse response filter of the NI PXI 5922A[1] (NI 2018) continuously reduce the remaining time interval where the Josephson voltage provides a quantized reference. The dashed lines indicate how the type-A uncertainty increases with frequency due to this effect. Sub-sampling circumvents this limitation and a very good agreement between AC quantum voltmeter and thermal transfer standard is found up to 100 kHz. Further details of the sub-sampling technique and an extensive discussion on type-B uncertainties are given in (Bauer *et al* 2021).

4.2. Resistance and current calibration (quantum calibrator)

Figure 16(a) shows two schematics how the AC quantum voltmeter could be extended to a 'quantum calibrator' (Lee *et al* 2016) for calibrating DC and AC currents and resistances, respectively. Such an extension is enabled by combining the AC-QVM with the reference resistance standard R_A. A current source is calibrated easily by measuring the voltage across this known resistance. Using a set of 1 Ω, 10 Ω, 100 Ω und 1 kΩ resistors, DC currents ranging between 20 µA and 1 A are covered. Type-A (relative) uncertainties are as low as 10^{-7} were achieved within 60 s, and the calibration results were in good agreement with conventional methods (Lee *et al* 2016). Examples demonstrating how accurate this method also works for AC has been published (Starkloff *et al* 2018); e.g. for frequencies from 30 Hz to 1 kHz and for currents from 1 mA to 20 mA, deviations are within ±5 µA A^{-1}, and ±20 µA A^{-1} when increasing the current to 2 A.

The availability of such a reference resistance standard makes it also possible to calibrate resistors. The schematic is shown in figure 16(b). A current source drives a current through the two resistors in series, the known one R_A and the one to be calibrated R_B. Thermal voltages and offsets are eliminated by current reversals. A multiplexer and the AC-QVM are used to precisely measure the voltages across the resistances successively. After an automated and well-timed series of four voltage measurements (each within 90 s), the resistance of R_B is given as voltage ratio times R_A (Lee *et al* 2016). With 1:10 scaling, four resistances R_A with values 1 Ω, 100 Ω, 10 kΩ, and 1 MΩ are sufficient to cover the resistance range from 1 Ω to 10 MΩ. Scaling can be performed with little

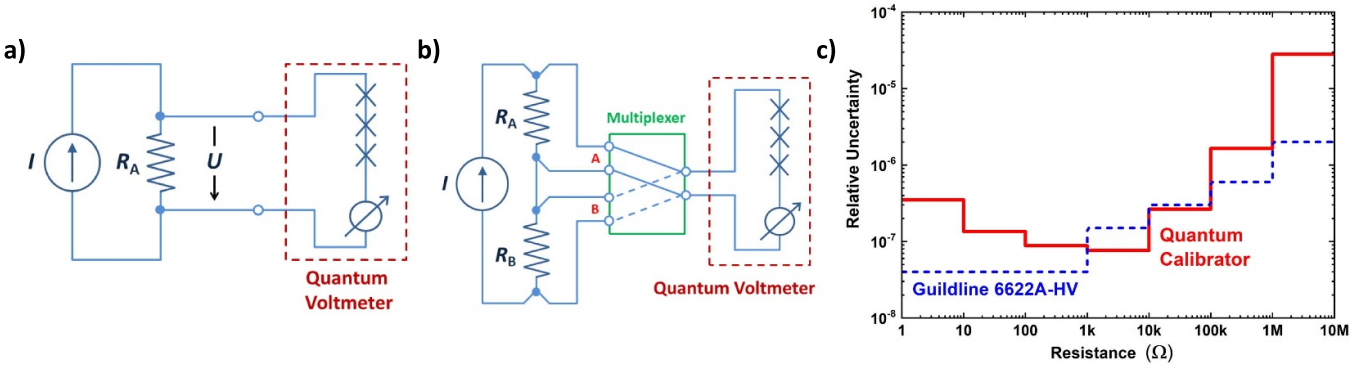

Figure 16. (a) and (b) Schematic setups using the quantum voltmeter for current and resistance calibrations, respectively. (c) Comparison of relative uncertainty levels ($k = 2$) for resistance calibrations from 1 Ω to 10 MΩ between a commercial resistance bridge and the AC-QVM.

uncertainty reduction and even 1:100 scaling can be used for crosschecks (Behr *et al* 2003, Lee *et al* 2016).

Figure 16(c) compares achievable uncertainties with the AC-QVM. As stable current source a Fluke calibrator[1] operated in the voltage range was used. Stable resistors from an oil bath were investigated and—as expected—the achieved results showed good uncertainties. Be aware that the relative uncertainties for the quantum calibrator in figure 16(c) slightly differ from that published in (Lee *et al* 2016) because we used resistors in an oil bath instead of common transportable standards and investigated more carefully all uncertainty components. In the 1 kΩ–10 kΩ resistance range, relative uncertainties below 10^{-7} (type-A, $k = 2$) are comparable to high-performance DC resistance bridges (Guildline 2016)[1]. Towards higher resistance values, leakage resistance of the AC-QVM set-up decreases the uncertainty. At resistance values below 100 Ω voltages diminish, and signal to noise reduces and uncertainty decreases again.

The AC-QVM ability to quickly switch between DC resistance and AC current calibrations was recently exploited to improve the short-time traceability of current shunts and, thus, to improve uncertainties of AC current calibrations to the 1 μA A^{-1} level ($k = 1$) (Ilic *et al* 2022).

4.3. DC measurements

As progress is ongoing in many metrological areas, JVS gain more importance outside common voltage or even electrical metrology. This is generally the case as soon as measurements being based or involving voltage measurement are aiming for uncertainties better than 1 part in 10^7. Zener references and precision voltmeters can provide five parts in 10^8 uncertainty but only with a lot of effort. Therefore, Kibble balance experiments in mass metrology involved JVS since early time, cf (Robinson and Schlamminger 2016). To ensure such improved uncertainties, a Josephson voltage standard was recently also embedded in single electron pump investigations (Stein *et al* 2015). In these experiments, JVS were used as quantum voltage measurement devices in a traditional way with polarity reversals. Presently, PJVS are gaining also interest as simple stable references. The stabilization of the output of a current source (Fan *et al* 2019) is an example which demonstrates that PJVS are suitable for this purpose. Even though offset voltages from thermal EMFs were not cancelled by polarity reversals, a relative stability of three parts in 10^9 at 5 V level was achieved. Such a stability is out of reach for Zener references.

5. Josephson synthesizer applications

The applications discussed in this chapter are almost exclusively based on JAWS. Even though PJVS were suggested as synthesizers when they were introduced (Hamilton *et al* 1995), many applications were and are limited in uncertainty due to the transients (Behr *et al* 2012). The remaining synthesizer application is a PJVS-based impedance bridge for identical, high value impedances e.g. 10 pF capacitances (Hagen *et al* 2017).

5.1. Spectrum analysis

The basic principle that uses a JVS as a reference for differential measurements (having been employed for DC intercomparisons since the introduction of JVSs for DC voltage in 1980s as well as for the quantum voltmeter (Behr *et al* 2007) to measure AC signals) can be extended for measuring multiple harmonics exploiting the programmable spectrum in a JAWS. Signal generators typically show a few harmonic components at their output and the setup in figure 17(a) improves the resolution for these smaller components by using a low noise and high bandwidth amplifier. The Josephson-based spectrum analyzer establishes the different amplitudes by nulling each of these components. Normally, this requires an iterative process to adjust the amplitude and phase angles of the larger harmonic components. The cornerstone of the Josephson-based spectrum analyzer is the spectral purity of the JAWS output, and we established a total harmonic distortion over the first 20 harmonics of −135 dB or 0.2 μV/V for an amplitude of 100 mV at 1 kHz using a classical method with a passive double-T notch filter and an amplifier, as shown in figure 17(b). The blue curve shows the spectrum at the output of the amplifier. The red curve includes the inverse transfer function of the double-T filter and the amplifier. The otherwise excellent-attenuation of the notch filter at the second harmonic, −5.6 dB

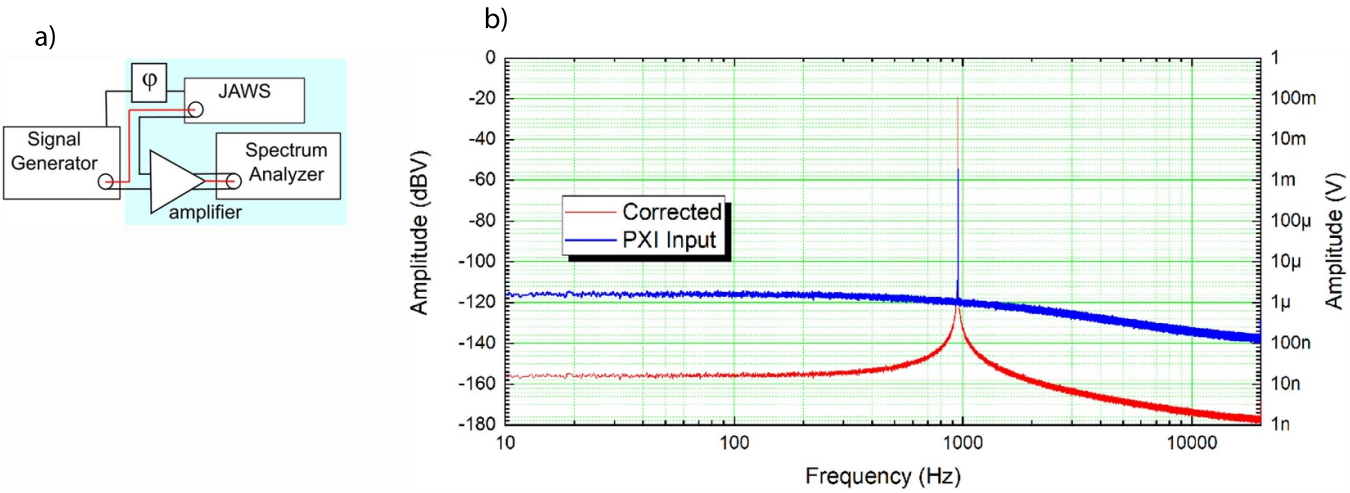

Figure 17. (a) Schematic setup as described in the text. (b) Frequency spectrum for a 100 mV JAWS sinewave at 1 kHz measured with a double-T notch filter and a low noise amplifier. The blue spectrum corresponds to the output of the amplifier while the red curve has been corrected for the transfer function of the notch filter and the amplifier.

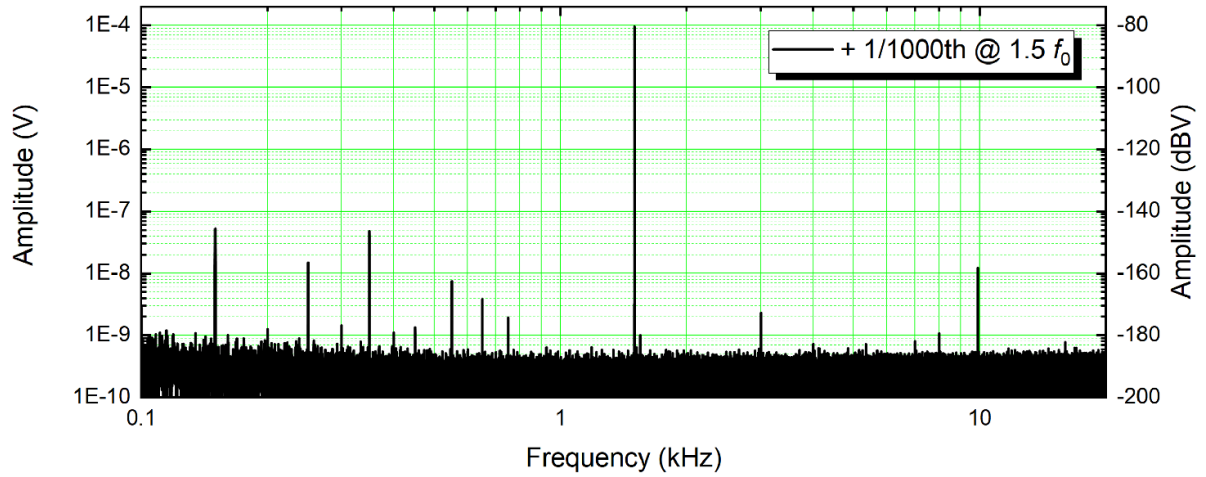

Figure 18. Single shot frequency spectrum from the Josephson based spectrum analyzer for a second JAWS signal consisting of two sine waves: 100 mV at 1 kHz plus 100 µV at 1.5 kHz.

as opposed to −10 dB for the conventional double-T configuration, limits the resolution of these measurements. The feasibility of the Josephson-based spectrum analyzer was established by using a second JAWS to generate a given spectrum and nulling its fundamental component (Palafox *et al* 2018). A single shot spectrum, acquired over less than 45 s, can reach noise floors of 0.5 nV, as shown in figure 18. In the measurement shown, we also demonstrated the 'infinite Q' of the cancellation method in the Josephson based spectrum analyzer. We generated a 100 mV tone at 1 kHz and 100 µV at 1.5 kHz, which is not harmonically related, but is not attenuated at all. Using commercial generators, the uncertainty of the measurement is dominated by their amplitude instability. If the generator shows instability in the frequency, this also contributes to the uncertainty of the measurement. For the instrument/generator investigated in (Palafox *et al* 2020), this can become 0.5 µV over 2 min.

5.2. µ*V-synthesizer*

In contrast to continuous wave operation, broad Shapiro steps are still generated in the pulse-mode operation regime when the pulse repetition rate is far below the characteristic frequency of the JJs. (Benz and Hamilton 1996). We practically used this feature for the first time to precisely synthesize very small DC and AC voltages. Such a precision microvolt synthesizer (Behr *et al* 2017) finds its application in calibrating nanovoltmeters (DC) or lock-in amplifiers (AC). The typical signal voltage range needed for the calibration of a nanovoltmeter is about $V = 10$ nV to $V = 100$ µV. We used a JAWS array with $N = 9000$ junctions and calculated the required ΣΔ-codes with a constant length of 128 Mbit and a fixed 5 GHz clock frequency. To generate these small voltages, no compensation signals (Benz *et al* 2001) are necessary (cf figure 12) and the ΣΔ-code amplitude $A_{\Sigma\Delta}$ could be as small

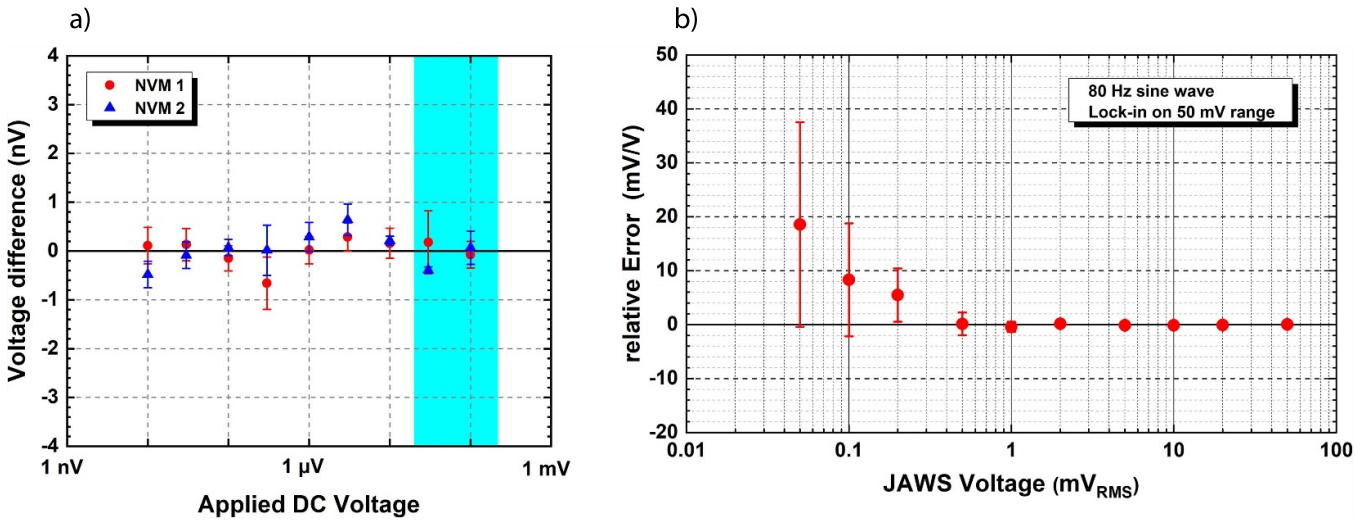

Figure 19. (a) Deviation from linearity for DC voltages in the μV-range measured with two digital nanovoltmeters (NVM) in the 10 mV range. The cyan-colored area indicates the typical voltage range for a single Josephson junction. (b) Deviation from linearity for 80 Hz AC voltages measured with a lock-in amplifier in the 50 mV range. The error bars indicate the measurement uncertainty ($k = 1$).

as 1.5×10^{-7} for a 10 nV DC voltage. Using a ternary PPG kept the JAWS setup simple, making it easy to reverse voltage polarity by sending either positive or negative pulse amplitudes. The results from the fully automated measurements are plotted in figure 19(a). All deviations are within ± 1 nV in the above-mentioned voltage range for two digital nanovoltmeters. The error bars indicate type-A uncertainties ($k = 1$).

By using a similar procedure, the generation of AC voltages was possible for the calibration of AC devices which are sensitive for small input signals. In (Behr *et al* 2017) a lock-in amplifier was calibrated in the range from 80 Hz to 100 kHz in a voltage range from 1 µV to 50 mV. Several features of this device like linearity, gain dependencies and influence of harmonic content were investigated. Figure 19(b) shows the deviation from linearity for an 80 Hz sine wave measured with a lock-in amplifier in the 50 mV range. At mV/V-level relative deviations are only visible for small amplitudes below 500 µV.

The minimum pulse repetition frequency applied for these experiments was only 540 Hz, far below the characteristic frequency of $f_c = 7.6$ GHz. Such a low frequency produces a minimum synthesized voltage of only $V_{JJ} = 1.1$ pV per JJ. The minimum possible voltage could be further explored by using the full available PPG memory of 512 Mbyte, by tuning down the clock frequency and by reducing the $\Sigma\Delta$-code amplitude. From a practical point of view, such a reduction is not required but shows the excellent suitability of the JAWS for this purpose. Uncertainties in the nanovolt level can be achieved within short measurement times and the fully automated calibration procedure makes it a useful tool for metrological applications.

5.3. IVD calibration

IVDs represent the actual standard to generate precise and reliable AC voltage ratios in metrology. As IVDs are relatively easy to self-produce and adapt to specific needs, they are used in a large variety of metrological measurements. Recently, they are also used to refer voltages of up to 120 V (unachievable with actual quantum voltage standards) to JAWS (Budovsky *et al* 2018). However, as these dividers are conventional technology, they must be calibrated from time to time to enable maximum accuracy for the measurements they are used for. Next to conventional techniques as bootstrapping (Sze 1968) and straddling (Hanke 1989), pulse driven JVS can be used for calibrating IVDs. Since pulse-driven JVS can generate any voltage signal with excellent accuracy, it is possible to realize highly accurate AC voltage ratios in a broad frequency range with two synchronized 100 mV JAWS systems (Herick *et al* 2018). In this way, the calibration of the divider is directly based on a quantum effect, thus benefiting from excellent performance, long term-stability, low noise and high precision of quantum effects. Note that at a 1:1 ratio, such calibration is very similar to a direct JAWS *versus* JAWS comparison, cf section 3.2.3.

The reference system JAWS1 supplies the input voltage V_i of the IVD to be calibrated (figure 20). To unload JAWS1 and to ensure best performance, the current required by the IVD is supplied by an additional buffer amplifier. JAWS2 is used to compensate the output voltage of the IVD at a ratio D_n. A detection transformer minimizes common-mode voltage effects while a pre-amplifier amplifies the signal difference and the sensitivity of the lock-in reading. Synchronization and phase setting are realized by an additional synthesizer. By raising the JAWS2 amplitude of a precisely known small amount, typically 1 µV/V or 100 nV, the sensitivity of the measurement setup is determined. Furthermore, such a signal is applied to set and check the phase setting of the lock-in amplifier.

The stability and noise level of the setup is analyzed by Allan deviation measurements for different configurations. Figure 21 shows such a measurement at 497 Hz for the in-phase and quadrature components. The blue and purple

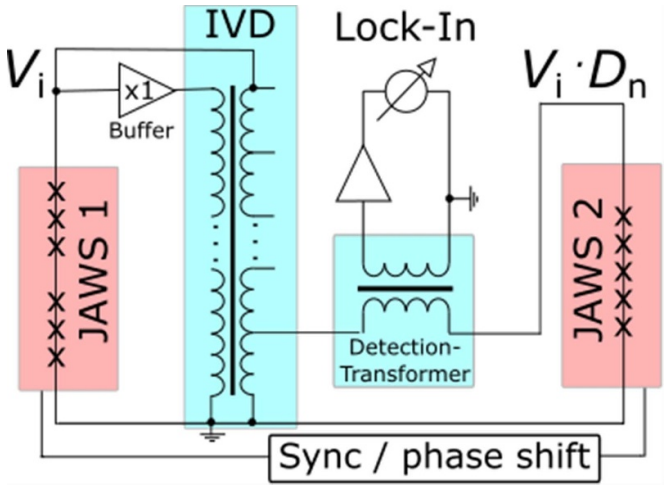

Figure 20. Schematic illustration of the measurement setup for the IVD calibration using two independently synchronized JAWS systems. JAWS1 is driving the IVD to be calibrated while JAWS2 is used to compensate and so measure the output voltage of the IVD at a ratio D_n. A detection transformer is used to minimize common-mode voltage effects and an amplifier is used to increase the combined signal and so the sensitivity of the lock-in amplifier reading. © 2018 IEEE. Reprinted, with permission, from (Herick *et al* 2018).

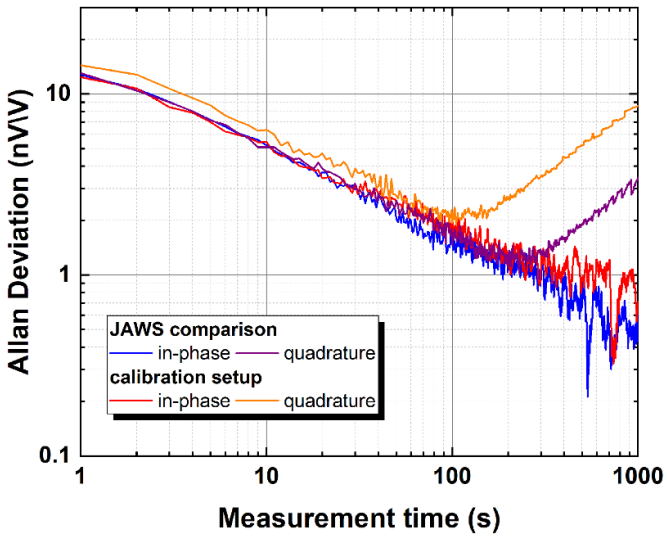

Figure 21. Allan deviation analysis at 497 Hz for the in-phase and quadrature components relative to the 100 mV_{rms} JAWS amplitude. The calibration setup is compared to a direct Josephson comparison (without buffer and IVD, cf figure 20). After 100 s all curves reach an uncertainty level of about 2 nV/V.

plots are corresponding to the direct JAWS comparison while the red and yellow lines are showing the results for the complete setup as shown in figure 20. The plot shows that the buffer amplifier starts drifting first, but does not significantly limit the type-A uncertainty of the setup which is in the range of 2 nV/V after a typical measurement time of 100 s.

The corrections, K_{in} and K_{qn}, of the IVD can be determined by a zero measurement, in which the output voltage at

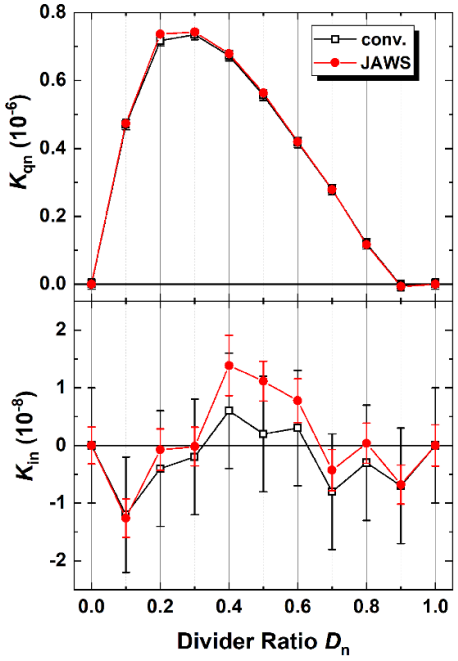

Figure 22. IVD calibration at 225 Hz for different divider ratios D_n. K_{in} and K_{qn} are the correction for the in-phase and quadrature component, respectively. The error bars indicate the total calibration uncertainties ($k = 2$).

the different taps of the IVD V_n of the IVD is compensated by voltage generated by JAWS2 and the difference signal is detected phase sensitive by a lock-in amplifier:

$$\frac{V_n}{V_i} = (D_n + K_{in} + j \cdot K_{qn}) .$$

As an example, figure 22 compares corrections, K_{in} and K_{qn}, which were extracted by JAWS at 100 mV level and the conventional bootstrap method at a voltage level of 1 V. At these low amplitudes the voltage dependence of the IVD is negligible. As expected, the in-phase corrections K_{in} are much smaller than the quadrature corrections, K_{qn}. Moreover, both methods are in good agreement, especially the in-phase calibrations agree very well within 1.1 parts in 10^8 for all divider ratios.

5.4. Josephson impedance bridges

The exact measurement of impedance plays an important role in many fields of science and engineering as well as in our daily life (e.g. capacitive touch screens). The different types of devices to measure electrical impedances developed over more than one century towards the two commonly used types of systems used nowadays. This are on the one hand impedance bridges based on IVD delivering the most precise performance up to now (Schurr *et al* 2009). On the other hand, so-called digital impedance bridges achieving uncertainties which are sufficient for many calibration purposes by giving a higher flexibility and the opportunity of automation. A special and highly accurate version of these digital bridges are using

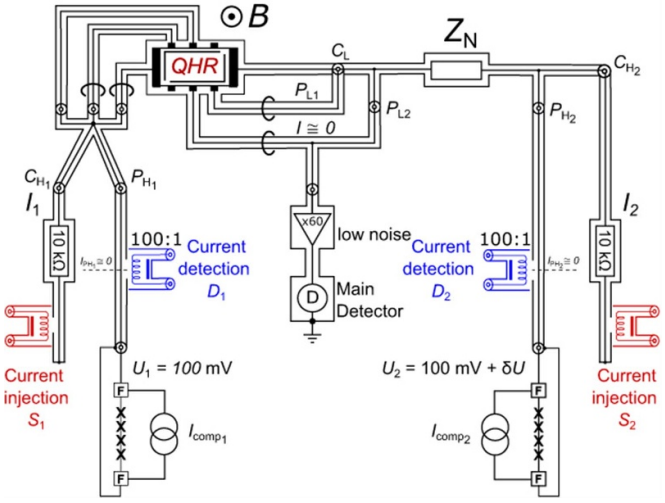

Figure 23. New Josephson impedance bridge after (Bauer *et al* 2021). Reproduced from (Bauer *et al* 2021). CC BY 4.0.

JVS for their potential definition. A detailed overview over the evolution of impedance bridges can be found in (Overney *et al* 2016).

The use of a JVS as reference for the potential definition offers low noise and infinite stability, hence giving low measurement uncertainties. Furthermore, the phase setting between the two needed voltages is much more flexible in contrast to the IVD based brides, which gives the ability to measure in the whole complex plane of impedance. First attempts to use JVS for impedance metrology were already carried out at PTB in 2010 (Lee *et al* 2010). Two synchronized PJVS systems with nominal output amplitudes of 1 V were used to measure the ratio of two 10 kΩ resistance standards in a two terminal-pair configuration. The uncertainties achieved by these measurements are in the range of a few parts in 10^8 for frequencies between 25 Hz and 10 kHz (Lee *et al* 2010). This impedance bridge was also used to make 1:1 and 10:1-measurements with 10 pF and 100 pF capacitance standards and amplitudes of up to 10 V. The achieved uncertainties are in the range between 0.9 and 81.1 parts in 10^8 in a frequency range between 500 Hz and 10 kHz (Hagen *et al* 2017). Due to the unavoidable transients and, hence, high harmonic content in a PJVS system (see figure 10), the uncertainty for a quadrature measurement (comparing unlike impedances R:1/(ωC)) is limited to some parts in 10^6 (Palafox *et al* 2012).

Accepting a lower amplitude this limitation can be circumvented by the usage of the high spectral purity of pulse-driven Josephson arrays. Moreover, the frequency range can be extended towards higher frequencies of 50 kHz or above. This type of a versatile and quantum-based impedance bridge is currently implemented by two institutes: one by a NIST-METAS collaboration (Overney *et al* 2016, 2020) and the other one by PTB. The latter was also used to link a 10 nF capacitance standard to the quantum Hall resistor (QHR) made from GaAs (Bauer *et al* 2017) and one from graphene (Bauer *et al* 2021). Figure 23 shows a schematic overview of the four-terminal pair impedance bridge combined with a QHR. With this setup, any type of impedance (Z_N) can be linked to the QHR. Those measurements can be carried out under relaxed experimental conditions by using a graphene based QHR, as it is intensively under investigation within the European metrology research project '**G**raphene **I**mpedance **Q**uantum **S**tandard' (GIQS) (GIQS 2022).

Recently the onsite comparison of two digital impedance bridges combined with a graphene quantum Hall standard has been published (Marzano *et al* 2022). One bridge the INRIM-POLITO digital impedance bridge using a polyphase digital sinusoidal waveform generator (Marzano *et al* 2020). The other one is PTBs Josephson impedance bridge as described in (Bauer *et al* 2021). The comparison between both systems agreed well within uncertainties which are about 2 parts in 10^7. Whereas the contribution of the Josephson impedance bridge is about 2 parts in 10^8. During this comparison a so-called triangle measurement was carried out using a ratio measurement between a resistance standard and a graphene quantum Hall standard as well as the quadrature measurements between a 10 nF capacitance standard and the two resistance standards. Every deviation of the result from 1 gives a hint to unaccounted systematic uncertainties. For the Josephson impedance bridge this deviation is 2 parts in 10^8 after subtracting the combined uncertainty of 1.6 parts in 10^8 ($k = 1$) and is currently under investigation (Marzano *et al* 2022).

Even though the absolute accuracy needs an improvement of about one order of magnitude to be on the level of the most accurate IVD bridges (Schurr *et al* 2009), the reproducibility is already in the range of few parts in 10^9 for frequencies around 1 kHz. For almost all industry needs those systems are already outperforming but on a metrology level and hence the representation of the unit farad based on the QHR/impedance improvements are still need and the target of all further research.

Beside impedance metrology Josephson impedance bridges are useful tools also to investigate two electrical quantum standards the Josephson voltage standard and the quantum Hall impedance standard. For the JVS the QLR can be measured with a resolution of few parts in 10^9. For a quantum Hall device, the plateau shape can be measured by investigating the change in detector reading with respect to the magnetic field when the QHR is measured against a resistance or capacitance standard. The latter is a quadrature measurement which is easy possible with digital impedance bridges and offers a lower noise compared to a measurement using a resistance standard as reference (Bauer *et al* 2020a, Bauer *et al* 2021).

5.5. Johnson noise thermometry

Johnson noise thermometers (JNTs) exploit the relation between the voltage noise across a resistor R (caused by the thermal motion of charge carriers) and its thermodynamic temperature (Johnson 1928, Nyquist 1928). The temperature T is then derived from the power spectral density (PSD) of the resistor vie the relation $S_T = 4k_BTR$, where k_B is the Boltzmann constant. Due to the small voltage noise levels of about 1.27 nV/$\sqrt{\text{Hz}}$ for a 100 Ω sensor resistor at room temperature, sensitive amplifier electronics and measurement

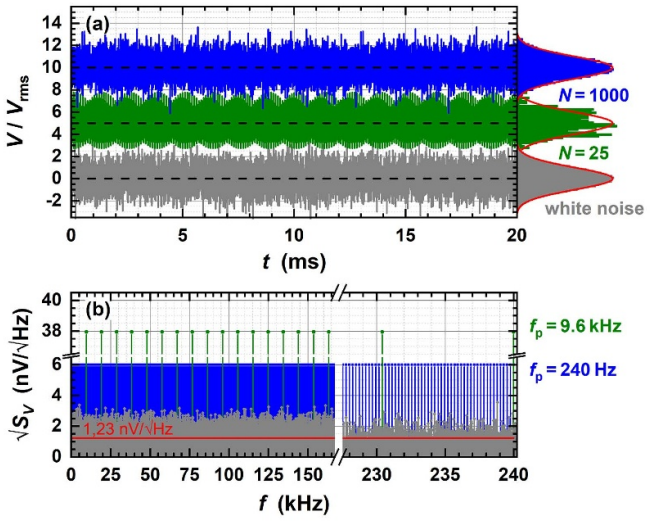

Figure 24. Comparison of different noise signals. In (a) the time signal, normalised to the rms voltage, of white and pseudo-noise with different tone numbers N and $V_{\mathrm{rms}} = 0.6\ \mu\mathrm{V}$ is sketched. Both waveforms with $N = 25$ and 1000 are shifted in positive y-direction. The three red lines represent Gaussian fit functions of the respective amplitude distribution. (b) Shows the voltage noise $\sqrt{S_V}$ of the signals from (a). The red line shows the thermal noise level for $R = 100\ \Omega$ and $T = 273.16$ K.

techniques are required to perform temperature measurements at μK/K-level (Coakley and Qu 2017, Flowers-Jacobs *et al* 2017, Qu *et al* 2017, 2019).

To date, the most accurate noise thermometer is based on the switching correlator design in combination with a quantum voltage noise source (QVNS), which is based on pulse-driven JJ arrays and generates a calculable reference pseudo noise (Flowers-Jacobs *et al* 2017, Qu *et al* 2017). In this QVNS thermometer, two identical amplifier channels measure the resistor's voltage noise simultaneously in cross-correlation. Every 100 s the electronics switches to the reference noise of the QVNS operating at the same noise level to overcome the limitations caused by instabilities and nonlinearities of the measurement electronics. This process is repeated over several hours, and the temperature is then derived from the ratio of the sensor and the reference pseudo noise. Since the voltage noise of the sensor is relatively low, the maximum number of JJ in the QVNS can be reduced to about 20 or even less (Nam *et al* 2003, Benz *et al* 2011).

The QVNS typically generates a voltage noise consisting of N equal-amplitude random phase harmonics (typically $N \geqslant 1000$) of a single sinusoid and frequency f_{p}. If the phases relation between all tones is appropriate, the synthesized signal resembles the behavior of white noise in the time domain (White and Benz 2008), which is sketched in figure 24(a). In the frequency domain however, the power is concentrated only in the tone frequency bins unlike 'true' white noise where the PSD is constant over the bandwidth studied. As a result, intermodulation distortions (IMD) caused by nonlinearities in the JNT electronics may affect the pseudo-noise and the thermal noise of the sensor differently, thus distorting the temperature measurement. Therefore, the choice of the pseudo waveform pattern must be made carefully. It has been shown that if the tone amplitudes are small enough (or, in other words, the tone density is maximized at a given noise level and the pseudo-noise consists only of odd harmonic tones), differences due to nonlinearity effects between white and pseudo-noise become negligible (Qu *et al* 2015).

At PTB, the concept for the JNT measurement electronics and its calibration is approached differently. For this purpose, a novel system, the dual-mode auto-calibrating resistance thermometer (DART) has been developed, which combines resistance and Johnson noise thermometry in one instrument (cf (Drung and Kraus 2021) for more details). The highly linear and stable signal path amplification of the DART in combination with a sophisticated measurement procedure and data analysis allows the temperature to be determined directly from the measured PSD of the sensor resistor without the need for permanent comparison with a QVNS reference noise during temperature measurements. Infrequent calibrations of the system against electrical quantum standards are sufficient to operate the thermometer over extended periods and wide temperature ranges. In the following, we present the reader with some very important milestones regarding the calibration concept of the DART as well as gain linearity investigations of a DART prototype.

Unlike the AC coupled amplifiers typically used in the QVNS thermometer, the DART employs a DC coupled amplifier to deduce the temperature also via the measured sensor's resistance (Drung and Kraus 2021). For this reason, the calibration of the thermometer must not only be carried out in the AC range with use of multitone waveforms, but also in DC, and a corresponding calibration concept for the DART has been developed in recent years. Figure 25(a) shows an example of the JAWS signal required to calibrate the DART (Drung *et al* 2022). During the calibration the DC gain is deduced from the mean values of the positive and negative voltage plateau of the square wave. The calibration requires higher voltage levels compared to the typical output voltages of a QVNS. Therefore, typically more JJ (up to 9000) are required like in the typical JAWS. The frequency-dependent AC gain is then deduced from the tone amplitudes of the superimposed synthetic noise (Kraus *et al* 2021, Drung *et al* 2022).

The spectrum of the synthetic noise is displayed in figure 25(b). We use a so-called low-distortion multitone waveform consisting of a small number of tones with tone phases of either 0 or π and with slightly increasing tone spacing, minimizing the effect of IMD on the tone amplitudes during the calibration. Quite specifically, for special sets of tone frequencies, neither harmonics nor third-order IMD coincide with any of the N tones. Hence, the effect of odd higher-order IMD products is also significantly suppressed. This has been discussed and demonstrated in detail in (Kraus *et al* 2021) by comparing the calibration results obtained with low-distortion and odd-harmonic multitones of equal tone number.

An example calibration of the AC gain for a prototype DART signal path, consisting of an amplifier and an ADC is shown in figure 26. Here, the calibration signal of figure 25(b) is applied to the signal path. The total gain of the signal path

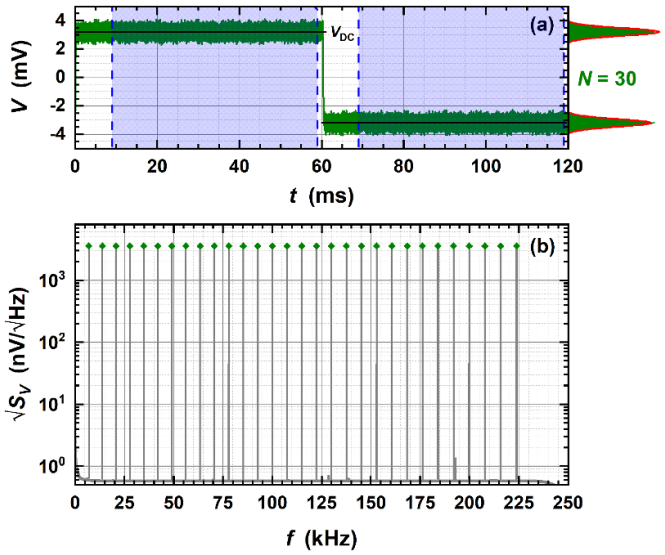

Figure 25. Time and frequency domain representation of the DART calibration signal. (a) Shows the signal synthesized by the JAWS versus time t over a complete period. The signal is a superposition of a synthetic noise consisting of 30 low-distortion tones and a ± 3.6 mV square-wave having finite rise and fall times with a time constant of 500 µs. The red curves represent Gaussian fits of the amplitude distribution. Blue solid lines mark the mean values of the plateaus $\pm V_{DC} = 3.6$ mV. The data used for calibrating AC and DC gain is shaded in blue. (b) Shows the corresponding voltage noise of the superimposed low-distortion multitone.

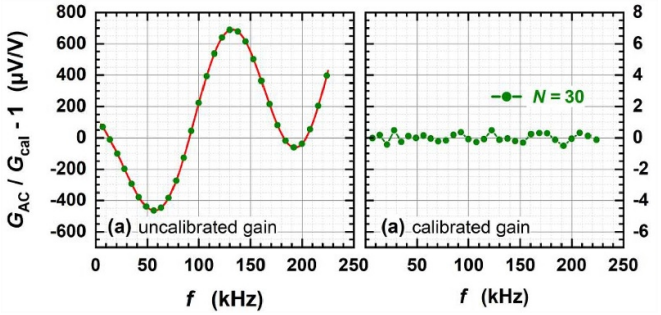

Figure 26. Relative deviation of the AC gain G_{AC} of a DART prototype signal path consisting of amplifier and ADC from the calibrated gain G_{cal} (a) before and (b) after applying a suitable calibration function to the tone amplitudes of the low-distortion multitone from figure 25(b). The red solid line marks the calibration curve deduced from DC to 225 kHz. Reproduced from (Kraus *et al* 2021). © IOP Publishing Ltd All rights reserved.

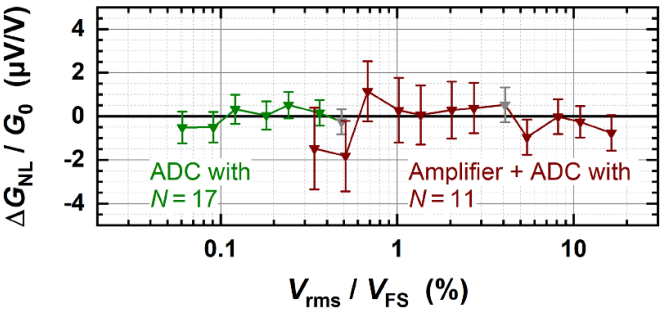

Figure 27. Relative deviation of the gain nonlinearity $\Delta G_{NL}/G_0$ as a function of the total amplitude V_{rms} of the tones at the ADC input normalized to the ADC's full-scale input range V_{FS} for different signal path configurations. ΔG_{NL} is deduced from the relative gain changes for the reference amplitude highlighted in grey and the amplitude under investigation. The error bars represent type-A uncertainties ($k = 1$). In the green and brown configurations, a high-frequency dither tone and a broadband noise dither, respectively, were implemented in the generated waveform of the JAWS to improve the linearity of the overall gain. Reproduced from (Kraus *et al* 2021). © IOP Publishing Ltd All rights reserved.

G_{AC} is defined in the frequency domain as the ratio of the amplified tone amplitudes measured by the ADC and the known signal amplitudes at the amplifier input. As can be seen in figure 26(a), the gain deviates from -500 µV/V to 700 µV/V up to 225 kHz. A suitable calibration fit shown in red is then applied to deduce the calibration parameters from the known tone amplitudes. The residuals of the fit shown in figure 26(b) remain within ± 1 µV/V. During temperature measurements with the DART, the calibration parameters will be used to calibrate the thermal noise spectra of the sensor resistor. Then, the temperature can be directly deduced from the noise level of the calibrated spectra (Kraus *et al* 2021, Drung *et al* 2022).

In addition to calibrating the signal path gain, the JAWS was also used to investigate the gain linearity of a prototype DART signal path with low-distortion multitones (Kraus *et al* 2021), which is another critical step towards realizing a practical noise thermometer without the need for permanent recalibration. One major result of these investigations is shown in figure 27. Here, the nonlinearity of the signal path gain ΔG_{NL} with respect to the low-frequency (extrapolated to DC) signal gain G_0 is quantified by applying low-distortion multitones with different rms amplitudes to the input of the signal path, which resembles noise thermometer measurements performed at different virtual temperatures. The study shows that without dither the gain linearity of the investigated signal path at low amplitudes is dominated by the ADC. With dither applied to the synthesized JAWS signal, the remaining nonlinearity is strongly reduced to better than ± 2 µV/V between $V_{rms}/V_{FS} = 0.34\%$ and 16.31%, limited by amplifier noise at low signal amplitudes. Additional measurements focused on the influence of an applied offset voltage on the gain linearity (Kraus *et al* 2021). Finally, with the help of JAWS, the most recent investigations have shown that the gain fluctuations of a DART prototype over a period of 19 d are within ± 2 µV/V, representing another important milestone in the DART development (Drung *et al* 2022).

6. Conclusions and outlook

We have summarized the main applications advanced at PTB in the past ten years. Even 60 years after the discovery of the Josephson effect, intensive worldwide efforts are ongoing to establish quantum standards for AC metrology in diverse application fields. The development of improved Josephson series arrays for PJVS and JAWS opened a toolbox for new AC applications and became the next chapter in this exciting story

about applications of the Josephson effect in metrology. Significant progress in fabrication technology presented in section 2 has enabled routine fabrication of binary 20 V arrays and pulse-driven arrays for up to 4 V_{rms} systems. In section 3 we have presented application areas and summarized comparison results. Metrological applications based on measurement methods, so far solely on PJVS, are reviewed in section 4. These applications demonstrate PTB's pioneering developments to extend the frequency range of the AC quantum voltmeter to 100 kHz, as well as towards DC and AC current and resistance metrology based on the AC-QVM. The synthesis of completely quantum-defined AC voltages with pulse-driven arrays has led to very promising Josephson synthesizer applications (section 5). We have demonstrated spectrally pure waveforms, JAWS for IVD calibrations, JAWS phase standards, Josephson impedance bridges and an excellent QVNS for Johnson noise thermometry.

More exciting applications lie ahead on the road to quantum-based metrology. A world-wide effort for better uncertainties at frequencies towards 1 MHz is visible, and even to extend JAWS into the GHz-regime (Brevik *et al* 2020). The aim to generate higher AC voltages with JAWS is also very challenging due to the complex operation using short current pulses—in section 2 we have discussed several promising options for being successful. Finally, we like to stress that a high-voltage and high-bandwidth JAWS would represent the ultimate Josephson voltage standard. However, specific precision metrology applications will always benefit from specific solutions out of the Josephson voltage standard toolbox.

Data availability statement

All data that support the findings of this study are included within the article (and any supplementary files).

Acknowledgments

The authors would like to thank Johannes Kohlmann, Peter Hinze, Thomas Weimann, Rüdiger Wendisch, Rolf Gerdau, Kathrin Störr and Franz Müller from the Josephson array fabrication team. They are grateful to Susanne Gruber, Gerd Muchow, Torsten Stöcker and Michael Busse for technical support. Furthermore, we would also like to thank Jinni Lee, Karsten Kuhlmann, Torsten Funck, Bernd Schumacher, Susanne Weimann, Christian Krause, Dietmar Drung and Jürgen Schurr (all PTB), Ilya Budovsky (NMIA), Björnar Karlsen (JV), Damir Ilic (FER), Alexander Katkov (VNIIM), Jan Kucera (CMI), Jaani Nissilä (VTT), Marco Schubert (Supracon), Stéphane Solve (BIPM) for valuable discussions and conventional calibrations which led to the applications reviewed in this paper.

ORCID iDs

Stephan Bauer https://orcid.org/0000-0001-6242-2223
Ralf Behr https://orcid.org/0000-0002-5480-443X
Oliver Kieler https://orcid.org/0000-0001-5193-8910
Marco Kraus https://orcid.org/0000-0002-7592-9493
Hao Tian https://orcid.org/0000-0001-5341-6841
Yoawaret Pimsut https://orcid.org/0000-0001-9210-6512
Luis Palafox https://orcid.org/0000-0001-7663-856X

References

Albis 2022 PD20X1 28 Gb/s photodiode with integrated lens (Switzerland: Albis Optoelectronics AG) (available at: www.albisopto.com/albis_product/pd20x1/)

Amagai Y, Maruyama M, Sakamoto N, Shimazaki T, Yamamori H, Fujiki H and Kaneko N 2018 Sampling measurement of a 20-V RMS sine wave using an inductive voltage divider and an AC-programmable Josephson voltage standard *Conf. on Precision Electromagnetic Measurements (CPEM 2018)* (https://doi.org/10.1109/CPEM.2018.8500812)

Baek B, Dresselhaus P D and Benz S P 2006 Co-sputtered amorphous Nb_xSi_{1-x} barriers for Josephson-junction circuits *IEEE Trans. Appl. Supercond.* **16** 1966–70

Bardalen E, Karlsen B, Malmbekk H, Kieler O, Akram M N and Ohlckers P 2017 Packaging and demonstration of optical-fiber-coupled photodiode array for operation at 4 K *IEEE Trans. Compon. Packag. Manuf. Technol.* **7** 1395–401

Bardalen E, Karlsen B, Malmbekk H, Kieler O, Akram M N and Ohlckers P 2018 Reliability study of fiber-coupled photodiode module for operation at 4 K *Microelectron. Reliab.* **81** 362–7

Bardalen E, Nissilä J, Fordell T, Karlsen B, Kieler O and Ohlckers P 2020 Bipolar photodiode module operated at 4 K *IEEE 8th Electronics System-Integration Technology Conf. (ESTC)* (*Tönsberg, Norway, 15–18 September*) (https://doi.org/10.1109/ESTC48849.2020.9229695)

Bauer S *et al* 2021 A four-terminal-pair Josephson impedance bridge combined with a graphene-quantized Hall resistance *Meas. Sci. Technol.* **32** 065007

Bauer S, Behr R, Beug F, Herick J, Kieler O, Kölling A, Moser H and Schmidt M 2023 Realizing a phase standard based on pulse-driven Josephson arrays *Metrologia* submitted

Bauer S, Behr R, Hagen T, Kieler O, Lee J, Palafox L and Schurr J 2017 A novel two-terminal-pair pulse-driven Josephson impedance bridge linking a 10 nF capacitance standard to the quantized hall resistance *Metrologia* **54** 152–60

Bauer S, Pimsut Y, Behr R, Kieler O, Kruskopf M, Palafox L, Lee J and Schurr J 2020a AC quantum hall resistance combined with a four-terminal pair pulse-driven Josephson impedance bridge *Conf. on Precision Electromagnetic Measurements (CPEM2020)* (https://doi.org/10.1109/CPEM49742.2020.9191895)

Bauer S, Schmidt M, Beug F, Herick J, Kieler O and Behr R 2020b Realization of a phase reference system based on two synchronized pulse-driven Josephson voltage standards *Conf. on Precision Electromagnetic Measurements (CPEM2020)* (https://doi.org/10.1109/CPEM49742.2020.9191747)

Behr R, Funck T, Schumacher B and Warnecke P 2003 Measuring resistance standards in terms of the quantized Hall resistance with a dual Josephson voltage standard using SINIS Josephson arrays *IEEE Trans. Instrum. Meas.* **52** 521–3

Behr R, Kieler O, Kohlmann J, Müller F and Palafox L 2012 Development and metrological applications of Josephson arrays at PTB *Meas. Sci. Technol.* **23** 124002–20

Behr R, Kieler O, Lee J, Bauer S, Palafox L and Kohlmann J 2015 Direct comparison of a 1 V Josephson arbitrary waveform synthesizer and an AC quantum voltmeter *Metrologia* **52** 528–37

Behr R, Kieler O and Schumacher B 2017 A precision microvolt-synthesizer based on a pulse-driven Josephson voltage standard *IEEE Trans. Instrum. Meas.* **66** 1385–90

Behr R and Palafox L 2021 An AC quantum voltmeter for frequencies up to 100 kHz using sub-sampling *Metrologia* **58** 025010
Behr R, Palafox L, Ramm G, Moser H and Melcher J 2007 Direct comparison of Josephson waveforms using an AC quantum voltmeter *IEEE Trans. Instrum. Meas.* **56** 235–8
Benz S P, Burroughs C J and Dresselhaus P D 2000 Low harmonic distortion in a Josephson arbitrary waveform synthesizer *Appl. Phys. Lett.* **77** 1014
Benz S P, Burroughs C and Dresselhaus P D 2001 AC coupling technique for Josephson waveform synthesis *IEEE Trans. Appl. Supercond.* **11** 612–6
Benz S P, Dresselhaus P D and Burroughs C J 2011 Multitone waveform synthesis with a quantum voltage noise source *IEEE Trans. Appl. Supercond.* **21** 681–6
Benz S P and Hamilton C A 1996 A pulse-driven programmable Josephson voltage standard *Appl. Phys. Lett.* **68** 3171–3
Benz S P and Waltman S B 2014 Pulse-bias electronics and techniques for a Josephson arbitrary waveform synthesizer *IEEE Trans Appl. Supercond.* **24** 1400107
Benz S P, Waltman S B, Fox A E, Dresselhaus P D, Rüfenacht A, Howe L A, Schwall R E and Flowers-Jacobs E 2015b Performance improvements for the NIST 1 V Josephson arbitrary waveform synthesizer *IEEE Trans. Appl. Supercond.* **25** 1400105
Benz S P, Waltman S B, Fox A E, Dresselhaus P D, Rüfenacht A, Underwood J M, Howe L A, Schwall R E and Burroughs C J 2015a One-volt Josephson arbitrary waveform synthesizer *IEEE Trans. Appl. Supercond.* **25** 1300108
BIPM 2019 *The International System of Units (SI)* 9th Sèvres BIPM (available at: https://bipm.org/utils/common/pdf/si-brochure/SI-Brochure-9-EN)
Brevik J A, Boaventura A S, Babenko A A, Castellanos-Beltran M A, Flowers-Jacobs N E, Fox A E, Hopkins P F, Dresselhaus P D, Williams D F and Benz S P 2020 Cryogenic calibration of the RF Josephson arbitrary waveform synthesizer *Conf. on Precision Electromagnetic Measurements (CPEM 2020)* (https://doi.org/10.1109/CPEM49742.2020.9191746)
Brevik J A, Flowers-Jacobs N E, Fox A E, Golden E B, Dresselhaus P D and Benz S P 2017 Josephson arbitrary waveform synthesis with multilevel pulse *IEEE Trans Appl. Supercond.* **27** 1301707
Brevik J, Lee D, Fox A, Peng Y, Babenko A, Campbell J, Dresselhaus P, Quinlan F and Benz S 2022 Bipolar waveform synthesis with an optically driven Josephson arbitrary waveform synthesizer *IEEE Trans. Appl. Supercond.* **32** 1–8
Budovsky I, Georgakopoulos D and Benz S P 2018 AC voltage measurements up to 120 V with a Josephson arbitrary waveform synthesizer and an inductive voltage divider *Conf. on Precision Electromagnetic Measurements* (*Paris, France*) (https://doi.org/10.1109/CPEM.2018.8501176)
Burroughs C J, Benz S P and Dresselhaus P D 2003 AC Josephson voltage standard error measurements and analysis *IEEE Trans. Instr. Meas.* **52** 542–4
Coakley K and Qu J 2017 Spectral model selection in the electronic measurement of the Boltzmann constant by Johnson noise thermometry *Metrologia* **54** 204–17
Dresselhaus P D, Elsbury M, Olaya D, Burroughs C J and Benz S P 2011 10 V programmable Josephson voltage standard circuits using NbSi-barrier junctions *IEEE Trans. Appl. Supercond.* **21** 693–6
Drung D and Kraus C 2021 Dual-mode auto-calibrating resistance thermometer: a novel approach with Johnson noise thermometry *Rev. Sci. Instrum.* **92** 034901
Drung D, Kraus M and Krause C 2022 Calibration of the dual-mode auto-calibrating resistance thermometer with few-parts-per-million uncertainty *Meas. Sci. Technol.* **33** 015008
Elsbury M M, Dresselhaus P D, Bergren N F, Burroughs C J, Benz S P and Popovic Z 2009 Broadband lumped-element integrated *N*-way power dividers for voltage standards *IEEE Trans. Microw. Theory and Tech.* **57** 2055–63
Fan I, Behr R, Drung D, Krause C, Götz M, Pesel E and Scherer H 2019 Externally referenced current source with stability down to 1 nA/A at 50 mA *IEEE Trans. Instrum. Meas.* **68** 2129–35
Filipski P S, Kinard J R, Lipe T E, Tang Y and Benz S P 2008 Correction of systematic errors due to the voltage leads in an AC Josephson voltage standard *IEEE Trans. Instrum. Meas.* **58** 853–8
Flowers-Jacobs N E, Pollarolo A, Coakley K J, Fox A E, Rogalla H, Tew W L and Benz S P 2017 A Boltzmann constant determination based on Johnson noise thermometry *Metrologia* **54** 730–7
Flowers-Jacobs N E, Rüfenacht A, Fox A E, Dresselhaus P D and Benz S P 2016a 2 volt pulse-driven Josephson arbitrary waveform synthesizer *2016 Conf. on Precision Electromagnetic Measurements (CPEM)* (https://doi.org/10.1109/CPEM.2016.7540601)
Flowers-Jacobs N E, Rüfenacht A, Fox A E, Dresselhaus P D and Benz S P 2016b Two-volt Josephson arbitrary waveform synthesizer using Wilkinson dividers *IEEE Trans. Appl. Supercond.* **26** 1400207
Flowers-Jacobs N E, Rüfenacht A, Fox A E, Dresselhaus P D and Benz S P 2020 Calibration of an AC voltage source using a Josephson arbitrary waveform synthesizer at 4 V *Conf. on Precision Electromagnetic Measurements (CPEM 2020)* (https://doi.org/10.1109/CPEM49742.2020.9191787)
Flowers-Jacobs N E, Rüfenacht A, Fox A E, Waltman S E, Schwall R E, Brevik J A, Dresselhaus P D and Benz S P 2019 Development and applications of a four-volt Josephson arbitrary waveform synthesizer *IEEE Int. Superconductive Electronics Conf. (ISEC 2019)* (https://doi.org/10.1109/ISEC46533.2019.8990937)
Georgakopoulos D, Budovsky I, Benz S P and Gubler G 2019 Josephson arbitrary waveform synthesizer as a reference standard for the measurement of the phase of harmonics in distorted waveforms *IEEE Trans. Instrum. Meas.* **68** 1927–34
GIQS 2022 Home (available at: www.ptb.de/empir2019/giqs/home/)
Guildline 2016 Guildline 6622A series operation manual (ManualsLib)
Hagen T, Palafox L and Behr R 2017 A Josephson impedance bridge based on programmable Josephson voltage standards *IEEE Trans. Instrum. Meas.* **66** 1539–45
Hamilton C A, Burroughs C J and Kautz R L 1995 Josephson D/A converter with fundamental accuracy *IEEE Trans. Instrum. Meas.* **44** 4–6
Hanke R 1989 An improved straddling method with triaxial guards for the calibration of inductive voltage dividers at 1592 Hz *IEEE Trans. Instrum. Meas.* **38** 974–8
Herick J, Bauer S, Behr R, Beug M F, Kieler O F O and Palafox L 2018 Calibration of an inductive voltage divider using pulse-driven Josephson arrays *Conf. on Precision Electromagnetic Measurements (CPEM 2018)* (https://doi.org/10.1109/CPEM.2018.8500789)
Herick J, Palafox L, Bardalen E, Bauer S, Behr R, Karlsen B, Kieler O and Malmbekk H 2020 Realization of an opto-electronic bias for pulse-driven Josephson voltage standards at PTB *Conf. on Precision Electromagnetic Measurements Denver (USA)* (https://doi.org/10.1109/CPEM49742.2020.9191913)
Ilic D, Heinrich A, Meisner J and Behr R 2022 Calibration of a precision current measurement system for high AC voltages using an AC quantum voltmeter *Metrologia* **59** 055004

Ireland J *et al* 2017 Josephson arbitrary waveform system with optoelectronic drive *ISEC 2017 Proc. Int. Supercondive Electronics Conf.* (*Sorrento, Italy*, *12–16*)
Ireland J, Williams J, Kieler O, Behr R, Houtzager E, Hornecker R and van den Brom H 2019 An optoelectronic pulse drive for quantum voltage synthesizer *IEEE Trans. Instr. Meas.* **68** 2066–71
Jeanneret B, Rüfenacht A, Overney F, van den Brom H E and Houtzager E 2011 High precision comparison between a programmable and a pulse-driven Josephson voltage standard *Metrologia* **48** 311–6
Johnson J B 1928 Thermal agitation of electricity in conductors *Phys. Rev.* **32** 97–109
Karlsen B, Bardalen E, Nissilä J, Kieler O, Palafox L, Behr R, Malmbekk H, Akram M and Ohlckers P 2020 High-speed pulsation of a cryogenically operable bipolar photodiode module for the Josephson arbitrary waveform synthesizer *Conf. on Precision Electromagnetic Measurements* (*Denver, USA*) (https://doi.org/10.1109/CPEM49742.2020.9191751)
Karlsen B, Kieler O, Behr R, Nguyen T A T, Malmbekk H, Akram M N and Ohlckers P 2019 Pulsation of InGaAs photodiodes in liquid helium for driving Josephson arrays in AC voltage realization *IEEE Trans. Appl. Supercond.* **29** 1200308
Kieler O F O, Landim R P, Benz S P, Dresselhaus P D and BurroughsJr C J 2008 AC/DC transfer standard measurements and generalized compensation with the AC Josephson voltage standard *IEEE Trans. Instrum. Meas.* **57** 791–6
Kieler O F, Behr R, Schleussner D, Palafox L and Kohlmann J 2013b Precision comparison of sine waveforms with pulse-driven Josephson arrays *IEEE Trans. Appl. Supercond.* **23** 1301404
Kieler O F, Behr R, Wendisch R, Bauer S, Palafox L and Kohlmann J 2015 Towards a 1 V Josephson arbitrary waveform synthesizer *IEEE Trans. Appl. Supercond.* **25** 1400305
Kieler O *et al* 2019 Optical pulse-drive for the pulse-driven AC Josephson voltage standard *IEEE Trans. Appl. Supercond.* **29** 1200205
Kieler O, Behr R and Kohlmann J 2013a Development of a pulse-driven AC Josephson voltage standard at PTB *ISEC 2013 Proc. 14th Int. Superconductive Electronics Conf.* (*Cambridge, USA*) pp 59–61
Kieler O, Behr R, Wendisch R and Kohlmann J 2017 Arrays of stacked SNS Josephson junctions for pulse-driven Josephson voltage standards *EUCAS 2017 13th European Conf. on Applied Superconductivity* (*Geneva, Switzerland*, *17–21 September*)
Kieler O, Iuzzolino R and Kohlmann J 2009 Sub-μm SNS Josephson junction arrays for the Josephson arbitrary waveform synthesizer *IEEE Trans. Appl. Supercond.* **19** 230–3
Kieler O, Wendisch R, Gerdau R-W, Weimann T, Kohlmann J and Behr R 2021 Stacked Josephson junction arrays for the pulse-driven AC Josephson voltage standard *IEEE Trans. Appl. Supercond.* **31** 1100705
Kim M-S, Cho H, Chayramy R and Solve S 2020 Measurement configurations for differential sampling of AC waveforms based on a programmable Josephson voltage standard: effects of sampler bandwidth on the measurements *Metrologia* **57** 065020
Kim M-S, Kim K-T, Kim W-S, Chong Y and Kwon S-W 2010 Analog-to-digital conversion for low-frequency waveforms based on the Josephson voltage standard *Meas. Sci. Technol.* **21** 115102
Kraus M, Drung D, Behr R, Palafox L, Kieler O, Bauer S and Herick J 2020 Measurement and analysis of high-frequency voltage errors in the Josephson arbitrary waveform synthesizer *Meas. Sci. Technol.* **31** 125003
Kraus M, Drung D, Krause C, Behr R and Palafox L 2021 Linearity measurements of critical Johnson noise thermometer components with low-distortion multitones from a Josephson arbitrary waveform synthesizer *Meas. Sci. Technol.* **32** 065006
Kraus M, Kieler O, Behr R, Herick J, Bauer S, Palafox L and Ahlers F 2018 Frequency-dependent verification of the quantum accuracy of a quantum voltage noise source *2018 Conf. on Precision Electromagnetic Measurements (CPEM 2018)*
Kučera J, Kováč J, Palafox L, Behr R and Vojáčková L 2020 Characterization of a precision modular sinewave generator *Meas. Sci. Technol.* **31** 064002
Kürten Ihlenfeld W G and Landim R P 2016 Investigations on extending the frequency range of PJVS based AC voltage calibrations by coherent subsampling *Conf. on Precision Electromagnetic Measurements (CPEM 2016)* (https://doi.org/10.1109/CPEM.2016.7539732)
Landim R P, Benz S P, Dresselhaus P D and Burroughs C J 2008 Systematic-error signals in the AC Josephson voltage standard: measurement and reduction *IEEE Trans. Instrum. Meas.* **57** 1215–20
Lee J, Behr R, Palafox L, Schubert M, Starkloff M and Böck A C 2013 An ac quantum voltmeter based on a 10 V programmable Josephson array *Metrologia* **50** 612–22
Lee J, Behr R, Schumacher B, Palafox L, Schubert M, Starkloff M, Böck A C and Fleischmann P M 2016 From AC quantum voltmeter to quantum calibrator *Conf. on Precision Electromagnetic Measurements (CPEM 2016)* (https://doi.org/10.1109/CPEM.2016.7540470)
Lee J, Schurr J, Nissilä J, Palafox L and Behr R 2010 The Josephson two-terminal-pair impedance bridge *Metrologia* **47** 453–9
Marzano M, Ortolano M, D'Elia V, Müller A and Callegaro L 2020 A fully digital bridge towards the realization of the farad from the quantum Hall effect *Metrologia* **58** 015002
Marzano M, Pimsut Y, Kruskopf M, Yin Y, Kraus M, D'Elia V, Callegaro L, Ortolano M, Bauer S and Behr R 2022 PTB–INRIM comparison of novel digital impedance bridges with graphene impedance quantum standards *Metrologia* **59** 065001
Mueller F, Behr R, Palafox L, Kohlmann J, Wendisch R and Krasnopolin I 2007 Improved 10 V SINIS series arrays for applications in AC voltage metrology *IEEE Trans. Appl. Supercond.* **17** 649–52
Mueller F, Behr R, Weimann T, Palafox L, Olaya D, Dresselhaus P D and Benz S P 2009 1 V and 10 V SNS programmable voltage standards for 70 GHz *IEEE Trans. Appl. Supercond.* **19** 981–6
Müller F, Scheller T, Lee J, Behr R, Palafox L, Schubert M and Kohlmann J 2014 Microwave design and performance of PTB 10 V circuits for the programmable Josephson voltage standard *World J. Condens. Matter Phys.* **4** 107–22
Muller F, Scheller T, Wendisch R, Behr R, Kieler O, Palafox L and Kohlmann J 2013 NbSi barrier junctions tuned for metrological applications up to 70 GHz: 20 V arrays for programmable Josephson voltage standards *IEEE Trans. Appl. Supercond.* **23** 1101005
Nam S W, Benz S P, Dresselhaus P D, Tew W L, White D R and Martinis J M 2003 Johnson noise thermometry measurements using a quantized voltage noise source for calibration *IEEE Trans. Instrum. Meas.* **52** 550–4
NI 2018 NI PXI/PCI-5922 specification, PXI-5922 specifications—National Instruments (available at: ni.com)
Nissilä J *et al* 2021 Driving a low critical current Josephson junction array with a mode-locked laser *Appl. Phys. Lett.* **119** 032601
Nissila J, Šíra M, Lee J, Öztürk T, Arifovic M, de Aguilar J D, Lapuh R and Behr R 2016 Stable arbitrary waveform generator as a transfer standard for ADC calibration *Conf. on Precision Electromagnetic Measurements (CPEM 2016)* (https://doi.org/10.1109/CPEM.2016.7540454)
Nyquist H 1928 Thermal agitation of electric charge in conductors *Phys. Rev.* **32** 110–3

Overney F, Flowers-Jacobs N E, Jeanneret B, Rüfenacht A, Fox A E, Dresselhaus P D and Benz S P 2020 Dual Josephson impedance bridge: towards a universal bridge for impedance metrology *Metrologia* **57** 065014

Overney F, Flowers-Jacobs N E, Jeanneret B, Rüfenacht A, Fox A E, Underwood J M, Koffman A D and Benz S P 2016 Josephson-based full digital bridge for high-accuracy impedance comparisons *Metrologia* **53** 1045

Palafox L, Behr R, Nissilä J, Schurr J and Kibble B P 2012 Josephson impedance bridges as universal impedance comparators *Conf. on Precision Electromagnetic Measurements CPEM Digest* pp 464–5

Palafox L, Herick J, Bauer S, Kraus M, Kieler O and Behr R 2020 Applications of the Josephson based spectrum analyzer *Conf. on Precision Electromagnetic Measurements (CPEM)* (https://doi.org/10.1109/CPEM49742.2020.9191890)

Palafox L, Herick J, Behr R, Kieler O F O and Schubert M 2018 Josephson based spectrum analyzer *Conf. on Precision Electromagnetic Measurements (CPEM 2018)* (https://doi.org/10.1109/CPEM.2018.8500926)

Qu J F, Benz S P, Rogalla H, Tew W L, White D R and Zhou K 2019 Johnson noise thermometry *Meas. Sci. Technol.* **30** 112001

Qu J, Benz S P, Coakley K, Rogalla H, Tew W L, White D R, Zhou K and Zhou Z 2017 An improved electronic determination of the Boltzmann constant by Johnson noise thermometry *Metrologia* **54** 549–58

Qu J, Benz S P, Pollarolo A, Rogalla H, Tew W L, White D R and Zhou K 2015 Improved electronic measurement of the Boltzmann constant by Johnson noise thermometry *Metrologia* **52** 242–56

Robinson I A and Schlamminger S 2016 The watt or Kibble balance: a technique for implementing the new SI definition of the unit of mass *Metrologia* **53** A46

Rufenacht A, Burroughs C J, Benz S P, Dresselhaus P D, Waltrip B C and Nelson T L 2009 Precision differential sampling measurements of low-frequency synthesized sine waves with an AC programmable Josephson voltage standard *IEEE Trans. Instrum. Meas.* **58** 809–15

Rüfenacht A, Burroughs C J, Dresselhaus P D and Benz S P 2013 Differential sampling measurement of a 7 V RMS sine wave with a programmable Josephson voltage standard *IEEE Trans. Instrum. Meas.* **62** 1587–93

Rüfenacht A, Flowers-Jacobs N E and Benz S P 2018 Impact of the latest generation of Josephson voltage standards in ac and dc electric metrology *Metrologia* **55** S152–73

Rüfenacht A, Flowers-Jacobs N E, Fox A E, Burroughs C J, Dresselhaus P D and Benz S P 2016 Direct comparison of a pulse-driven Josephson arbitrary waveform synthesizer and a programmable Josephson voltage standard at 1 volt *Conf. on Precision Electromagnetic Measurements (CPEM)* (https://doi.org/10.1109/CPEM.2016.7540603)

Schubert M, Starkloff M, Lee J, Behr R, Palafox L, Boeck A C, Fleischmann P and May T 2015 An AC Josephson voltage standard up to the kHz range tested in a calibration laboratory *IEEE Trans. Instrum. Meas.* **64** 1620–6

Schurr J, Bürkel V and Kibble B P 2009 Realizing the farad from two ac quantum Hall resistances *Metrologia* **46** 619–28

Starkloff M, Bauer M, Schubert M, Lee J, Behr R, Palafox L, Schaidhammer L, Böck A C and Fleischmann P M 2018 The AC quantum voltmeter used for AC current calibrations *Conf. on Precision Electromagnetic Measurements (CPEM 2018)* (https://doi.org/10.1109/CPEM.2018.8500829)

Stein F *et al* 2015 Validation of a quantized-current source with 0.2 ppm uncertainty *Appl. Phys. Lett.* **107** 103501

Supracon AG 2022 Standards—Standards (available at: supracon.com)

Sze W C 1968 An injection method for self-calibration of inductive voltage dividers *J. Res. NBS* **72C** 49–59

Tian H 2022 Development of RF power dividers for highly integrated circuits of AC Josephson voltage standards *PhD thesis* submitted

Tian H, Kieler O F, Behr R, Gerdau R, Kuhlmann K and Kohlmann J 2021 Investigation of broadband Wilkinson power dividers for pulse-driven Josephson voltage standards *IEEE Trans. Appl. Supercond.* **31** 1–5

Tian H, Kieler O F, Behr R, Wendisch R, Gerdau R-W, Kuhlmann K and Kohlmann J 2020 Development of RF power dividers for the Josephson arbitrary waveform synthesizer *IEEE Trans. Appl. Supercond.* **30** 1100105

Underwood J M 2018 Uncertainty analysis for AC-DC difference measurements with the AC Josephson voltage standard *Metrologia* **56** 015012

van den Brom H E, Zhao D and Houtzager E 2016 Voltage lead errors in an AC Josephson voltage standard: explanation in terms of standing waves *Conf. On Precision Electromagnetic Measurements (CPEM 2016)* (https://doi.org/10.1109/CPEM.2016.7540666)

Watanabe M, Dresselhaus P D and Benz S P 2006 Resonance-free low-pass filters for the AC Josephson voltage Standard *IEEE Trans. Appl. Supercond.* **16** 49–53

White D R and Benz S P 2008 Constraints on a synthetic noise source for Johnson noise thermometry *Metrologia* **45** 93–101

Williams J M, Henderson D, Pickering J, Behr R, Müller F and Scheibenreiter P 2011 Quantum-referenced voltage waveform synthesiser *Sci. Meas. Technol. IET* **5** 167–74

Williams J M, Janssen T J B M, Palafox L, Humphreys D A, Behr R, Kohlmann J and Müööer F 2004 The simulation and measurement of the response of Josephson junctions to optoelectronically generated short pulses *Supercond. Sci. Technol.* **17** 815–8

Yamamori H, Ishizaki M, Shoji A, Dresselhaus P D and Benz S P 2006 10 V programmable Josephson voltage standard circuits using NbN/TiNx/NbN/TiNx/NbN double junction stacks *Appl. Phys. Lett.* **88** 042503

Yamamori H and Kohjiro S 2016 Fabrication of voltage standard circuits utilizing a serial–parallel power divider *IEEE Trans. Appl. Supercond.* 1400404

Zhao D, van den Brom H E and Houtzager E 2017 Mitigating voltage lead errors of an AC Josephson voltage standard by impedance matching *Meas Sci. Technol.* **28** 095004

Zhou K, Qu J and Benz S P 2015 Zero-compensation method and reduced inductive voltage error for the AC Josephson voltage standard *IEEE Trans Appl. Supercond.* **25** 1400806